minerals

MDPI

Article

Petrogenesis and Tectonic Setting of the Highly Fractionated Junye Granitic Intrusion in the Yiliu Tungsten Polymetallic Deposit, Guangdong Province, South China: Constraints from Geochemistry and Sr-Nd-Pb-Hf Isotopes

Tao Wu [1,2], Zhilong Huang [1,*], Mu Yang [3,*], Dexian Zhang [3], Jiawei Zhang [4] and Chen Wei [1]

1 State Key Laboratory of Ore Deposit Geochemistry, Institute of Geochemistry, Chinese Academy of Sciences, Guiyang 550081, China; wutao@mail.gyig.ac.cn (T.W.); weichen@mail.gyig.ac.cn (C.W.)
2 University of Chinese Academy of Sciences, Beijing 100049, China
3 School of Geoscience and Info-Physics, Central South University, Changsha 410083, China; dexian.zhang@csu.edu.cn
4 Guizhou Geological Survey, Bureau of Geology and Mineral Exploration and Development of Guizhou Province, Guiyang 550081, China; Jiaweizhang@live.cn
* Correspondence: huangzhilong@vip.gyig.ac.cn (Z.H.); yangmu@csu.edu.cn (M.Y.)

Received: 4 June 2020; Accepted: 13 July 2020; Published: 16 July 2020

Abstract: The Yiliu tungsten polymetallic deposit, located in the south central portion of the Nanling nonferrous metal metallogenic province in South China, is an area with common Yanshanian tectonothermal events. Early Yanshanian magmatism leads to the emplacement of voluminous tungsten-bearing granite intrusions, such as the Baoshan, Benggangling and Junye plutons, which are considered temporally and spatially associated with W-polymetallic mineralization in the Yiliu region. Here, we investigate the basic geological and petrological characteristics of the Junye granites, and present major and trace element geochemical data and bulk-rock Sr-Nd-Pb-Hf isotopic data to gain insight into the petrogenesis and tectonic setting of granitic intrusions in the region. The Junye granites are high-K calc-alkaline and metaluminous to weakly peraluminous [A/CNK = molar ratios of $Al_2O_3/(CaO + Na_2O + K_2O)$ = 0.97–1.02] with enrichment in SiO_2 (75.68–76.44 wt.%), relatively high total alkalis ($K_2O + Na_2O$ = 8.06–8.45 wt.%) with K_2O/Na_2O ratios ranging from 1.12 to 1.42, and moderate Al_2O_3 (12.62–13.00 wt.%), but low in P_2O_5 (<0.01 wt.%), MgO (0.02–0.04 wt.%), CaO (0.78–0.95 wt.%) and $Fe_2O_3{}^T$ (0.93–1.07 wt.%). They show spectacular tetrad effect REE (rare earth element) patterns with low ΣREE content (53.2–145.3 ppm), negative Eu anomalies (δEu = 0.09–0.17) and slight enrichment of LREEs (light rare earth elements) relative to HREEs (heavy rare earth elements). The granites are enriched in Rb (481–860 ppm), Th (16.2–46.1 ppm) and U (25.4–40.8 ppm) but depleted in Ba (1.0–5.8 ppm), Sr (11.1–23.4 ppm), P (9.5–26.7 ppm) and Ti (241–393 ppm). All geochemical features lead us to interpret the Junye granites as highly fractionated I-type granites. These granites underwent intense interaction between highly evolved magma and volatile-rich hydrothermal fluids during the late stage of formation, and accompanied fractional crystallization of biotite, plagioclase and accessory minerals, such as apatite, monazite and allanite. Additionally, the granites show uniform Nd isotopic ratios with calculated εNd (152 Ma) values of −8.28 to −8.91 and Nd model age (T_{DM2}) of 1645 to 1698 Ma, stable age-corrected initial Pb isotopic compositions with $(^{206}Pb/^{204}Pb)_i$ of 18.646–19.010, $(^{207}Pb/^{204}Pb)_i$ of 15.767–15.786 and $(^{208}Pb/^{204}Pb)_i$ of 39.113–39.159, respectively, and homogeneous Hf isotopic values yielding εHf (152 Ma) values from −6.9 to −9.5 with T_{DM2} ages of 1680 to 2214 Ma, collectively suggesting that the granitic magma was probably derived from the remelting of ancient infracrustal materials in the basement of the Nanling region. Consequently, we consider that the Junye granites are the products of partial melting of Paleoproterozoic infracrustal medium- to high-K metamorphic basaltic rocks in the Cathaysia Block,

which was caused by the underplating of coeval mantle basaltic magmas that provided abundant heat energy for melting in a tectonic setting, with lithospheric extension and thinning during the late Jurassic period.

Keywords: W-polymetallic deposit; Junye granites; fractionated I-type granite; Sr-Nd-Pb-Hf isotopes

1. Introduction

Mountain building in the Nanling mountains region, in the Cathaysia block of South China (Figure 1a,b), was accompanied by extensive magmatic activities, which resulted in the widespread emplacement of plutons during the Caledonian, Indosinian and Yanshanian tectonic events [1–5]. Among these, the Yanshanian magmatism was the most active and largest event (Figure 1b), producing numerous highly fractionated granitoids [6–12]. In the Nanling region, numerous tungsten–tin–molybdenum polymetallic deposits formed during the Mesozoic, which are believed to be closely related to the Yanshanian granites [13–18]. Since the 1990s, many studies relying on petrology, geochronology and major and trace elements as well as isotope geochemistry have been undertaken focusing on the emplacement ages, genetic types, magma sources and tectonic settings of granites in this region [19–25].

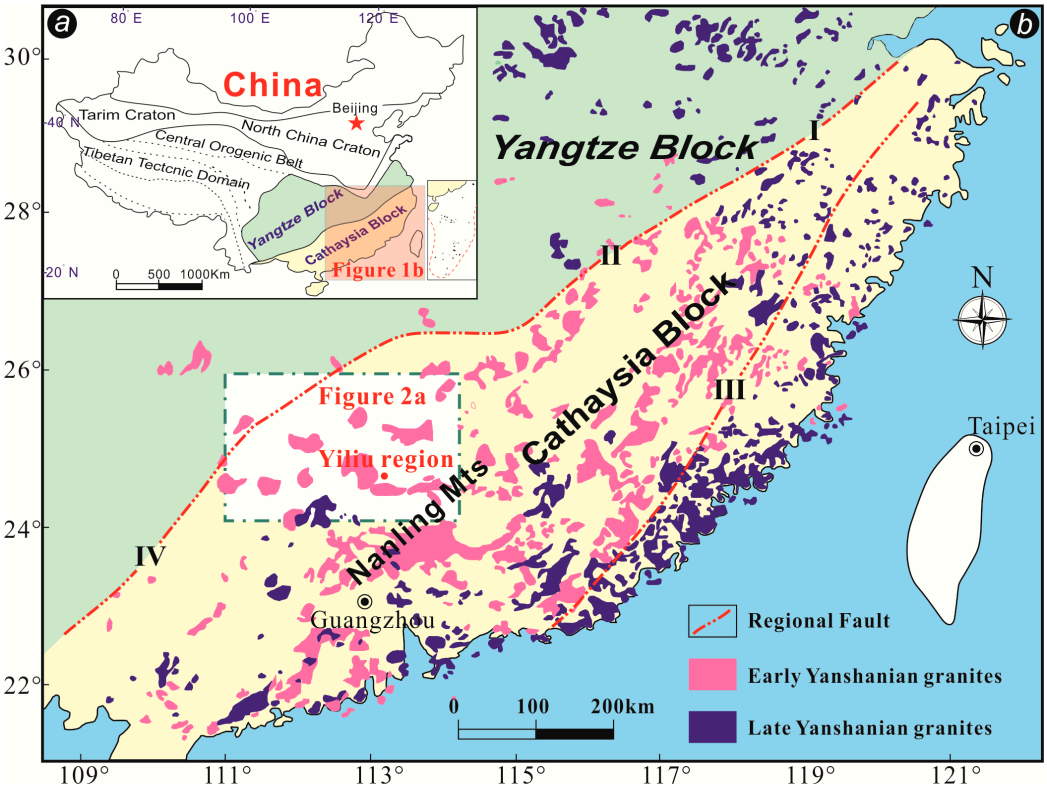

Figure 1. Geological sketch map of South China modified after Li et al. [11] and Li et al. [12], showing the geotectonic location of South China (**a**) and the distribution of Yanshanian granites (**b**). I: Jiangshan–Shaoxing fault; II: Pingxiang–Yushan fault; III: Zhenghe–Dapu fault; IV: Chenzhou–Linwu fault.

Geochronological studies have proven that granitoids with zircon U-Pb ages of 165–150 Ma dominate early Yanshanian magmatism in the Nanling region [12,19,23,26–28]. During this time, extension-induced deep crustal melting or underplating of mantle derived basaltic melts drove the formation of granitic magmatism in a tectonic setting of lithospheric extension and thinning [29–32].

The genetic classification and magma sources of these granitoids have always been controversial. This holds also true for the fractionated granites in the Nanling region, which may in fact exhibit some diagnostic features of I-type, S-type and A-type granite. For example, the genetic types of the Fogang granite pluton have been successively considered as S-type [33], A-type [34] and highly fractionated I-type [24]. Likewise, the Dadongshan granites have been interpreted as both S-type [35] and I-type [23]. Debates regarding magma sources include the view that the formation of granitic magmas in the Nanling region are the result of mantle-derived magmas reworking the crustal (meta-)sedimentary and/or meta-igneous rocks, with the mantle-derived magmas providing not only heat but also materials in this process [23,34,36,37]. Other researchers suggest that the underplating mantle magma, triggered by the subduction of the paleo-Pacific plate, only provides heat for the partial melting of the crustal materials without the involvement of mantle-derived components [12,38].

The Yiliu tungsten polymetallic deposit, located in the south central portion of the Nanling nonferrous metal metallogenic belt in the Cathaysia block, is an area with common Yanshanian tectonothermal events. (Figures 1b and 2a,b). Previous studies suggested that early Yanshanian granitic magmatism, which formed the Baoshan, Benggangling and Junye plutons (Figure 2b), possibly provided heat energy and ore-forming materials for tungsten polymetallic mineralization in the region [39–41]. Early Yanshanian granite plutons are the centre for a series of deposits, with high-temperature W-Sn deposits nearest the plutons, with adjacent medium-temperature Cu-Pb-Zn deposits, and with low-temperature Sb-Hg deposits at the greatest distance from the plutons [39,42]. Previous studies have not provided metallogenic ages for the deposits in the study area. Therefore, the genesis and tectonic evolution of granite in the region will aid in understanding the relationships between granitic magmatism and W-polymetallic mineralization. The major and trace element geochemistry for the Baoshan pluton have been studied by Liu and Lai [43], while research on magma sources and the tectonic setting of granite emplacement in the Yiliu area are still inconclusive. This paper provides zircon U-Pb ages, petrologic information, major and trace element abundances and Sr-Nd-Pb-Hf isotopic compositions in order to gain insight into the petrogenesis and the tectonic setting of the granitic intrusions. The outcomes will contribute to a fuller understanding of the source of granitic magma and provide further evidence regarding the contribution of the coeval mantle activity to the granitic magmatism in the Nanling region. It simultaneously enriches the theoretical system of the relationship between early Yanshanian granitic magmatism and W-polymetallic mineralization.

2. Geological Background

During the early Neoproterozoic period, the amalgamation of the Cathaysia Block, located to the southeast of the Jiangshan–Shaoxing and Pingxiang–Yushan faults, and the Yangtze Block in the northwest made up the South China Block (Figure 1b) [5,44–46]. The Nanling mountain region is mainly situated at the west central portion of the inland region in the western Zhenghe–Dapu fault of the Cathaysia Block (Figure 1b). The strata in the Nanling region is composed of a sedimentary cover and a metamorphic basement, the cover mostly consists of Devonian to Quaternary sedimentary rocks [47] and the basement consists mainly of Proterozoic meta-volcano-sedimentary, meta-sedimentary and meta-igneous rocks [11,48,49]. Extensive multistage magmatism in early Yanshanian leads to voluminous granitic plutons, such as the Dadongshan, Guidong, Fogang, Jiufeng, Xishan and Qitianling granites, in the central and southern Nanling area (Figures 1b and 2a). Notably, there are also numerous tungsten polymetallic deposits close to granitic plutons, including the Shizhuyuan W-Sn-Mo-Bi polymetallic deposit and the Yaogangxian, Dajishan and Xihuashan tungsten deposits [12].

The Yiliu W-polymetallic deposit, located in the Yiliu Town of Shaoguan City, Guangdong Province, China, is a typical skarn-type deposit. The exposed strata in the Yiliu region consists of Upper Devonian Tianziling Fm. (D_3t), Upper Devonian Maozifeng Fm. (D_3m) and Lower Carboniferous Menggongao Fm. (C_1ym) (Figure 2b), with the lithology of marble, marbleization-limestone, impure limestone and sandy shale. Anticline and NE-trending faults control the distribution of the igneous rocks and deposits (Figure 2b). The granitic intrusions, including the Baoshan, Benggangling and

Junye plutons, occur as stocks or dykes. The emplacement ages of 156.9 ± 2.4 Ma for the Baoshan granite and 151.9 ± 2.0 Ma for the Junye pluton based on zircon U-Pb dating (Mei et al., in preparation) suggest that the granites in the Yiliu region are the products of early Yanshanian magmatism.

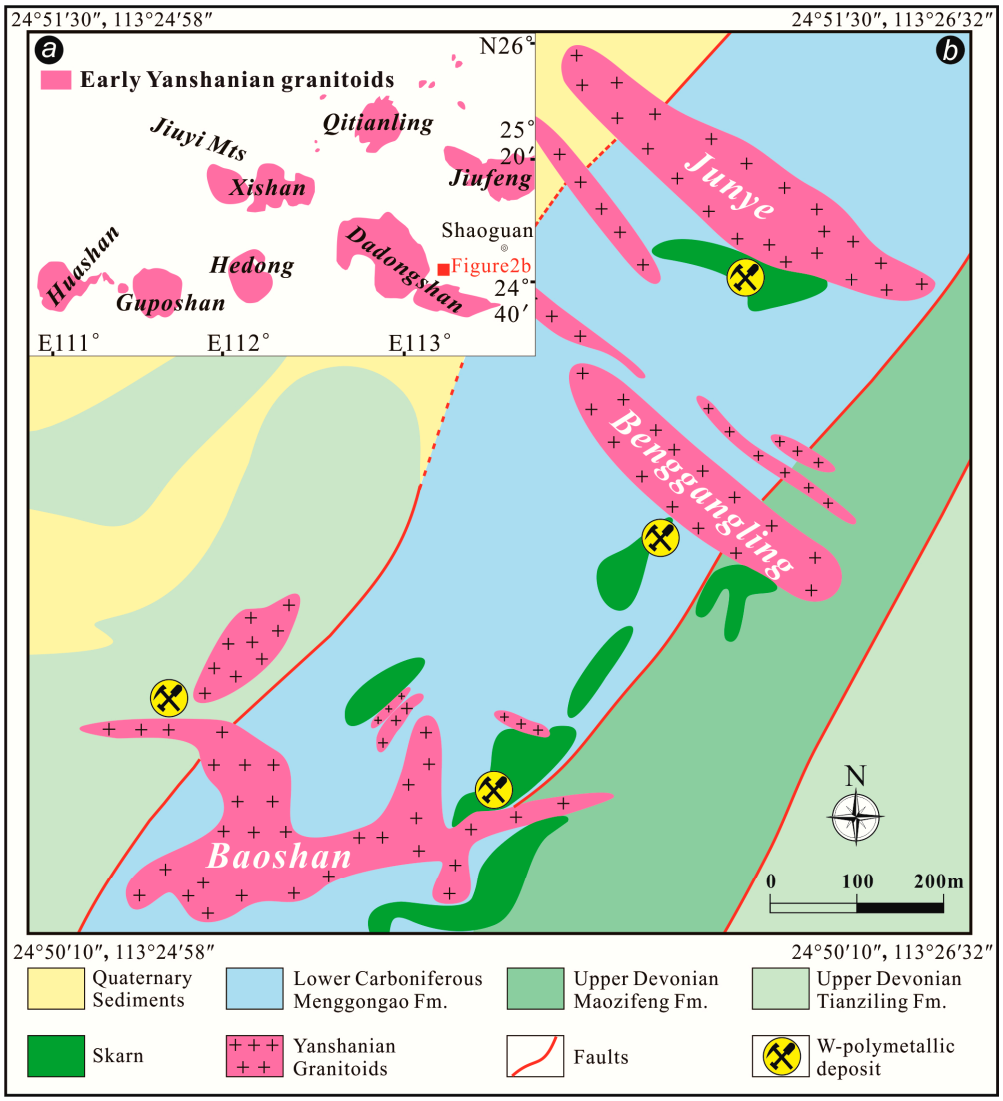

Figure 2. Simplified geological map of the western-middle part of the Nanling mountains region (**a**), modified after Zhu et al. [50], and the Yiliu region (**b**), exhibiting the distribution of early Yanshanian granites.

The NW-trending Junye granitic pluton, controlled by two NE-trending faults (Figure 2b), has mostly intruded into the limestone and the marbleization-limestone of the C_1ym Fm. The granites are grey-white to gray-black in colour and medium to fine-grained with a typical granite texture (Figure 3a–c). These granites are mainly composed of 20%–25% euhedral to subhedral plagioclase that shows polysynthetic twinning (Figure 3d), 30%–35% subhedral to anhedral K-feldspar with slight sericitization and carbonation (Figure 3d,f), 30%–35% anhedral granular quartz and 5%–8% euhedral flaky biotite (Figure 3e,f). Based on petrological and mineralogical characteristics, they are identified as biotite monzogranite. Moreover, in the vicinity of the contact zone between granites and carbonate rocks, wall-rock alterations, such as the formation of skarn and marble as well as silicification, usually occur near the orebodies, and this is accompanied by strong W, Cu, Pb and Zn mineralizations. The Junye granites are also rich in these ore-forming elements, especially W, which ranges from 533 to 781 ppm (Table 1).

Table 1. Bulk rock major (wt.%) and trace (ppm) element compositions of Junye granites.

Sample No.	JY-60-B2	JY-60-B3	JY-60-B5	JY-60-B6	JY-B6	JY-B10
SiO_2	76.44	75.74	76.12	75.68	76.13	76.15
TiO_2	0.03	0.05	0.05	0.05	0.04	0.06
Al_2O_3	12.76	12.80	12.80	13.00	12.62	12.62
Fe_2O_3	1.01	1.04	1.06	1.07	0.93	1.07
MnO	0.04	0.05	0.06	0.05	0.04	0.05
MgO	0.02	0.02	0.03	0.04	0.03	0.04
CaO	0.89	0.92	0.89	0.95	0.78	0.95
Na_2O	3.48	3.65	3.56	3.97	3.70	3.56
K_2O	4.93	4.53	4.89	4.46	4.60	4.50
P_2O_5	<0.01	<0.01	<0.01	<0.01	<0.01	<0.01
LOI	0.60	0.41	0.48	0.87	0.37	0.31
Total	100.20	99.23	99.95	100.14	99.27	99.33
K_2O/Na_2O	1.42	1.24	1.37	1.12	1.24	1.26
A/CNK	1.01	1.02	1.00	0.99	1.01	1.01
DI	94.15	93.76	94.07	93.89	94.68	93.58
Sc	3.38	3.18	4.51	4.00	3.29	3.34
Ti	241	296	343	330	293	393
P	9.51	15.7	21.9	19.7	18.2	26.7
V	0.35	0.65	0.88	0.98	0.56	0.68
Cr	2.51	1.67	2.00	2.08	2.76	3.66
Mn	254	338	376	413	300	391
Co	180	140	140	158	168	225
Ni	16.6	13.5	13.6	16.0	16.0	24.0
Cu	1.63	0.54	0.64	4.29	0.75	0.86
Zn	12.6	16.6	19.1	23.7	12.8	17.0
Ga	17.6	18.2	18.1	19.4	18.0	17.2
Rb	578	481	761	860	521	521
Sr	23.4	11.1	18.8	22.0	20.3	20.0
Y	73.4	34.1	63.8	57.1	34.8	61.8
Zr	74.2	41.3	152	37.4	39.8	80.8
Nb	22.4	16.2	22.9	17.6	13.4	15.9
Mo	0.35	0.28	1.90	1.03	0.36	0.57
Cd	0.02	0.02	0.05	0.08	0.02	0.03
Sn	7.47	14.7	15.8	16.4	12.0	18.4
Sb	0.35	0.74	0.72	0.82	1.09	0.80
Cs	18.5	54.9	69.3	77.7	44.2	77.5
Ba	5.08	1.01	5.69	5.79	2.40	2.39
La	4.52	11.1	10.1	8.24	6.74	19.0
Ce	11.0	25.0	25.4	20.7	16.2	48.0
Pr	1.52	3.03	3.34	2.88	2.12	6.77
Nd	6.08	10.5	12.6	11.0	7.92	26.8
Sm	2.56	2.92	3.68	3.66	2.60	8.38
Eu	0.09	0.12	0.23	0.17	0.10	0.27
Gd	3.92	3.02	4.21	4.23	2.93	7.95
Tb	0.92	0.59	0.83	0.85	0.61	1.45
Dy	6.84	3.98	5.66	5.66	4.15	9.10
Ho	1.70	0.93	1.32	1.28	0.96	1.92
Er	5.85	3.16	4.35	4.17	3.14	5.93
Tm	1.09	0.58	0.77	0.75	0.58	1.04
Yb	8.27	4.41	5.55	5.38	4.41	7.48
Lu	1.38	0.73	0.93	0.85	0.72	1.16
Hf	4.13	2.47	8.20	2.34	2.50	3.99
Ta	1.18	1.35	1.81	2.33	1.14	1.78
W	587	533	549	582	566	781
Tl	2.39	2.14	3.62	3.72	2.00	2.01
Pb	64.4	54.5	62.8	58.3	56.9	49
Th	16.2	30.5	41.3	33.5	17.6	46.1
U	40.6	40.8	33.4	25.4	38.6	32.7
ΣREE	55.7	70.1	79.0	69.8	53.2	145.3
LREE/HREE	0.86	3.03	2.34	2.01	2.04	3.03
La_N/Yb_N	0.39	1.81	1.31	1.10	1.10	1.82
δEu	0.09	0.12	0.17	0.13	0.11	0.10
10,000 Ga/Al	2.60	2.68	2.67	2.82	2.69	2.57

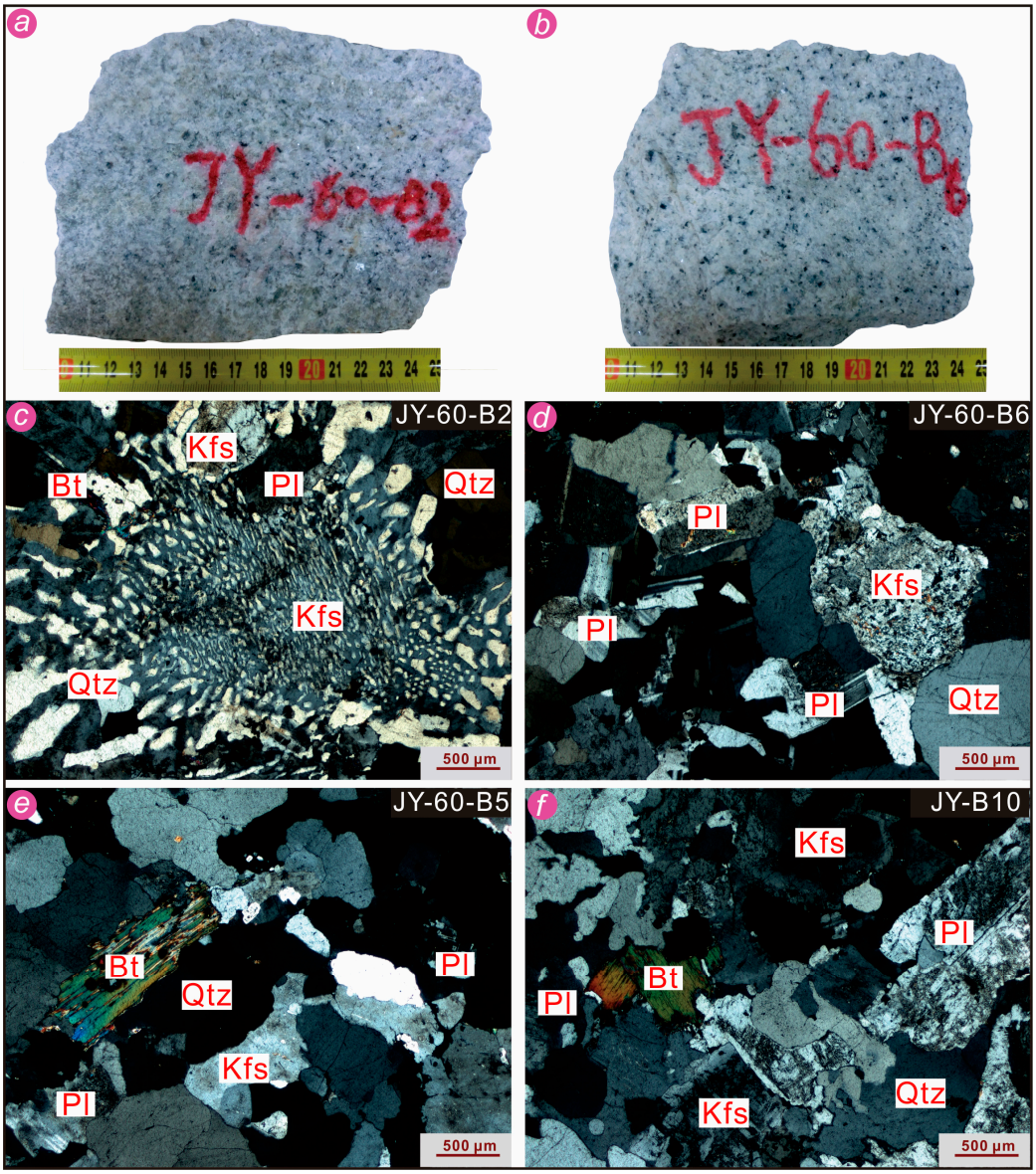

Figure 3. Photos of Junye pluton samples and microphotographs of thin sections under cross-polarized light: (**a**,**b**) typical biotite monzonitic granite; (**c**) graphic texture of intergrown quartz and K-feldspar; (**d**) twinned euhedral to subhedral plagioclase and slight argillization and carbonation of subhedral to anhedral K-feldspar; (**e**,**f**) euhedral flaky biotite and anhedral granular quartz. Abbreviations: Kfs = K-feldspar, Bt = biotite, Pl = plagioclase, Qtz = quartz.

3. Sampling and Analytical Methods

3.1. Sampling

Fresh samples of fifteen granites and four syenites were collected strictly following the principle of one sample every 30 m from north to south from the −60 m middle section of the pit in the Junye tungsten polymetallic deposit (Figure 2b, pithead coordinate: 113°26′12″ E, 24°51′06″ E). All samples were first characterized in hand specimen, and each sample was then cut off a small portion for study of the thin sections. After that, six typical granite samples were chosen for further analyses.

3.2. Major and Trace Elements Analyses

The least-altered six granite samples were carefully selected and sent to the Mineral Laboratory of ALS Co., Ltd (Guangzhou), China for major element analysis. These samples were respectively crushed in a steel jaw crusher and subsequently ground into powder with particle size less than 200 mesh (74 μm) using an agate mortar. Each prepared sample (0.66 g) was fused with a 12:22 lithium tetraborate–lithium metaborate flux which also included an oxidizing agent (lithium nitrate), and then poured into a platinum mould. Major element (SiO_2, TiO_2, Al_2O_3, TFe_2O_3, MnO, MgO, CaO, Na_2O, K_2O, P_2O_5) contents were determined by X-ray fluorescence (XRF) spectrometry (Malvern Panalytical, Almelo, Holland). SARM-45 (South African Bureau of Standards Private Bag X191 Pretoria Republic of South Africa 0001) and CCRMP (Canadian Certified Reference Materials Project) SY-4 were used as standards and the analytical uncertainties were generally within 5%.

The trace element compositions were analysed at the Guizhou Tongwei Analytical Technology Co., Ltd. The analytical procedure included sample pretreatment and instrument analysis. In brief, the first step was to dissolve about 50 mg of powder for each sample using a mixture of double distilled concentrated HNO_3-HF (1:4) in a Teflon bomb. The solutions were maintained for 3 d in an oven at a temperature of 185 °C, and then dried down to remove the HF. Next, the double-distilled concentrated HNO_3 and 1:1 HNO_3 were used to re-dissolve the sample residues, and then the samples were dried down again as in the first step. In the next step, the samples were dissolved in 3 mL 2N HNO_3 stock solution. Then, the sample solutions were diluted to 4000 times. Afterwards, internal spikes consisting of 6 ppb Rh, In, Re and Bi were added. The last step was to analyse the solutions after pretreatment on a Thermo Fisher iCAP RQ ICP–MS (Thermo Fisher Scientific Inc., Waltham, MA, USA) equipped with a Cetac ASX-560 AutoSampler (Teledyne CETAC Technologies, Ames, IA, USA). During the analytical process, USGS (United States Geological Survey) standard W-2a was used as reference standard, and cross tested with USGS standard BHVO-2 (Basalt, Hawaiian Volcanic Observatory) [51]. The analytical uncertainties of REE elements and other trace elements were generally within 3% and 5%, respectively. The ICP–MS procedures used in determining the trace elements followed the procedures of Eggins et al. [52] and Li et al. [53].

3.3. Bulk-Rock Sr-Nd-Pb-Hf Isotope Analyses

Whole-rock Sr-Nd-Pb-Hf isotopic analyses were performed at the Radiogenic Isotope Facility of the University of Queensland, Australia. The analytical processes generally consist of sample dissolution, separation of Sr, Nd, Pb and Hf, followed by ICP–MS analysis. Firstly, the methods and procedures for dissolving the samples are the same as those of trace element analysis described above. The next step was to perform column chemistry to separate Sr, Nd, Pb and Hf from the matrix, using separation procedures modified after Pin et al. [54], Deniel and Pin [55], and Mikova and Denkova [56]. Procedural blanks of Sr, Nd, Pb and Hf are approximately 65, 60, 50 and 16 pg, respectively. The ratios of $^{87}Sr/^{86}Sr$, $^{143}Nd/^{144}Nd$, $^{208}Pb/^{204}Pb$, $^{207}Pb/^{204}Pb$, $^{206}Pb/^{204}Pb$ and $^{176}Hf/^{177}Hf$ were determined on a Nu Plasma HR MC–ICP–MS (Nu Instruments, Wrexham, UK) with a modified CETAC ASX-110FR (Teledyne CETAC Technologies, Ames, IA, USA) auto sampler and a DSN-100 dissolvation nebulizing system (Nu Instruments, Wrexham, UK). The measured $^{87}Sr/^{86}Sr$, $^{143}Nd/^{144}Nd$, $^{208}Pb/^{204}Pb$, $^{207}Pb/^{204}Pb$, $^{206}Pb/^{204}Pb$ and $^{176}Hf/^{177}Hf$ ratios were corrected for mass fractionation using values of $^{86}Sr/^{88}Sr = 0.1194$, $^{146}Nd/^{144}Nd = 0.7219$, $^{205}Tl/^{203}Tl = 0.23875$ and $^{179}Hf/^{177}Hf = 0.7325$, respectively. During the process of analysis, NBS-987, JNdi-1, JMC-475 and NBS-981 standards were respectively used to monitor and calibrate the instrument drift of Sr, Nd, Hf and Pb, which generally yielded an average $^{87}Sr/^{86}Sr$ of 0.710248 ± 28 for NBS-987, $^{143}Nd/^{144}Nd$ of 0.512113 ± 9 for JNdi-1, $^{176}Hf/^{177}Hf$ of 0.282160 for JMC-475 and $^{208}Pb/^{204}Pb$ of 36.7071 ± 79, $^{207}Pb/^{204}Pb$ of 15.4944 ± 22, and $^{206}Pb/^{204}Pb$ 16.9370 ± 31 for NBS-981.

4. Analytical Results

4.1. Major Elements

Major element chemical compositions of typical samples from the Junye granitic intrusion are presented in Table 1. All samples have low values for loss on ignition (LOI) of 0.31–0.87 wt.%. As expected, all granites have high SiO_2 (75.68–76.44 wt.%), relatively high alkalis ($K_2O + Na_2O$ = 8.06–8.45 wt.%) with K_2O/Na_2O ratios ranging from 1.12 to 1.42, and moderate Al_2O_3 (12.62–13.00 wt.%), and low P_2O_5 (<0.01 wt.%), MgO (0.02–0.04 wt.%), CaO (0.78–0.95 wt.%) and TFe_2O_3 (0.93–1.07 wt.%). On the total alkalis–silica (TAS) diagram, the samples belong to the subalkaline series and plot in the field of granite (Figure 4a). The granite samples with K_2O contents of 4.46–4.93 wt.% plot in the area of high-K calc-alkaline series on the K_2O vs. SiO_2 diagram (Figure 4c). Aluminium saturation index (ASI = molar ratios of A/CNK) values of the samples range from 0.97 to 1.02. On the molar ratios of A/NK vs. A/CNK diagram, granites plot between metaluminous and peraluminous (Figure 4d). The Junye granites with high differentiation indices (DI = 93.58–98.40) plot in the field of differentiated calc-alkaline granites on the $(Al_2O_3 + CaO) / (FeO^T + Na_2O + K_2O)$ vs. $100 \times (MgO + FeO^T + TiO_2)/SiO_2$ diagram (Figure 4b).

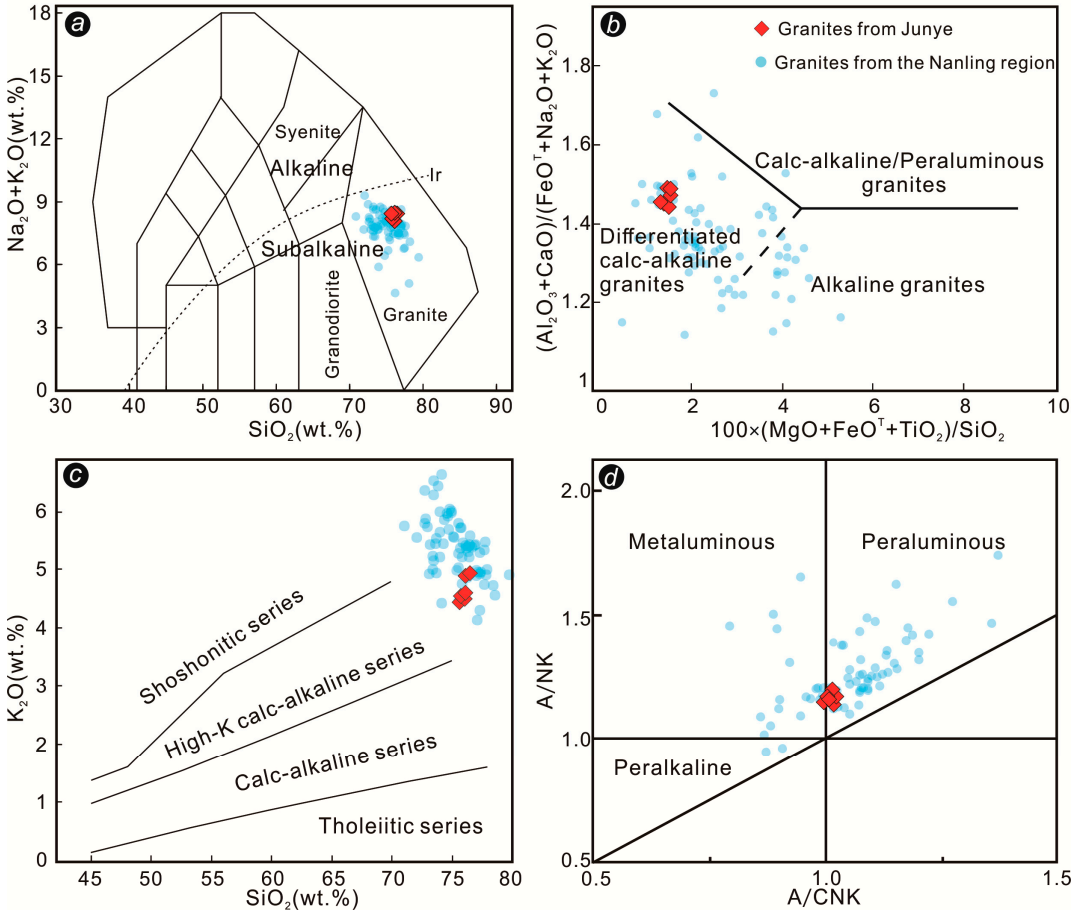

Figure 4. Discrimination diagrams based on major elements: (**a**) Total alkalis–silica (TAS) classification diagram for plutonic rocks (fields after middlemost. [57]) (**b**) Plots of $(Al_2O_3 + CaO)/(FeO^T + Na_2O + K_2O)$ vs. $100 \times (MgO + FeO^T + TiO_2)/SiO_2$ (fields after Sylvester. [58]) (**c**) K_2O vs. SiO_2 diagram (fields after Peccerillo et al. [59]) (**d**) A/NK vs. A/CNK diagram where A/NK = molar ratio $Al_2O_3/(Na_2O + K_2O)$, A/CNK = molar ratio $Al_2O_3/(CaO + Na_2O + K_2O)$ (fields after Maniar et al. [60]). The major element compositions for granites in the Nanling area are from Zhang et al. [35], Huang et al. [60], Yu et al. [38], Zhou et al. [16], Liu et al. [43] and Gu et al. [25].

Furthermore, all granite samples display medium to weak correlations between SiO_2 and some major oxides, showing increasing trend of K_2O (r = +0.74) and decreasing trends of Al_2O_3 (r = −0.62), CaO (r = −0.39), Na_2O (r = −0.80), Fe_2O_3 (r = −0.38) and TiO_2 (r = −0.53) with increasing SiO_2 (Figure 5). In general, the mineral compositions and major element characteristics of the Junye pluton are very similar to those of high silica granites including the Dajinshan [38], Dadongshan [23,35], Fogang [34], Baoshan [43], Xitian [16], Huashan and Guposhan plutons [25] in the Nanling mountains region.

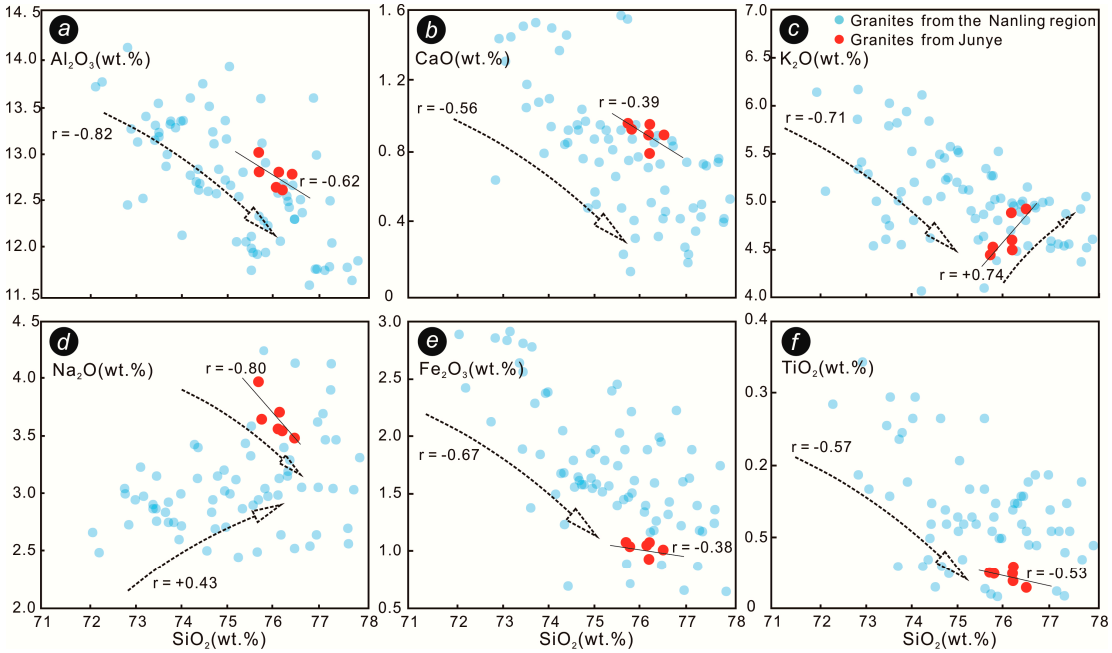

Figure 5. Harker diagrams that show Al_2O_3, CaO, K_2O, Na_2O, Fe_2O_3 and TiO_2 as a function of SiO_2. The compositions of major elements for granites in the Nanling area are from Zhang et al. [35], Huang et al. [23], Yu et al. [38], Zhou et al. [16], Liu et al. [43] and Gu et al. [25]. (**a**) Al_2O_3 vs. SiO_2, showing moderate to strong negative correlation between Al_2O_3 and SiO_2; (**b**) CaO vs. SiO_2, displaying moderate to weak negative correlation between CaO and SiO_2; (**c**) K_2O vs. SiO_2, showing strong negative correlation for granites from the Nanling region and strong positive correlation for granites from the Junye between K_2O and SiO_2; (**d**) Na_2O vs. SiO_2, displaying moderate positive correlation for granites from the Nanling region and strong negative correlation for granites from the Junye between Na_2O and SiO_2; (**e**) Fe_2O_3 vs. SiO_2, showing weak to moderate negative correlation between Fe_2O_3 and SiO_2; (**f**) TiO_2 vs. SiO_2, displaying moderate negative correlation between TiO_2 and SiO_2.

4.2. Trace Elements

The trace element compositions of the Junye pluton are given in Table 1. On the primitive mantle-normalized multiple trace element diagram (Figure 6a), granite samples are characterized by enrichments in Rb (481–860 ppm), Th (16.2–46.1 ppm) and U (25.4–40.8 ppm) as well as by extreme depletions in Ba (1.0–5.8 ppm), Sr (11.1–23.4 ppm), P (9.5–26.7 ppm) and Ti (241–393 ppm). In addition, all samples have relatively low contents of ΣREE ranging from 53.2 to 145.3 ppm. On the chondrite-normalized REE diagram (Figure 6b), the REE patterns display spectacular tetrad effects, which are possibly a consequence of intense interaction between highly evolved magma and volatile-rich (F, Cl, CO_2) hydrothermal fluids [61,62]. All granites show extremely negative Eu anomalies with δEu values of 0.09 to 0.17, and slight enrichments of LREEs relative to HREEs with $(La/Yb)_N$ ratios ranging from 0.39 to 1.82. It is noteworthy that the trace element compositions of Junye granites are similar to those of granites in the Nanling region, but are typically at the lower end of the spectrum for other samples (Figure 6).

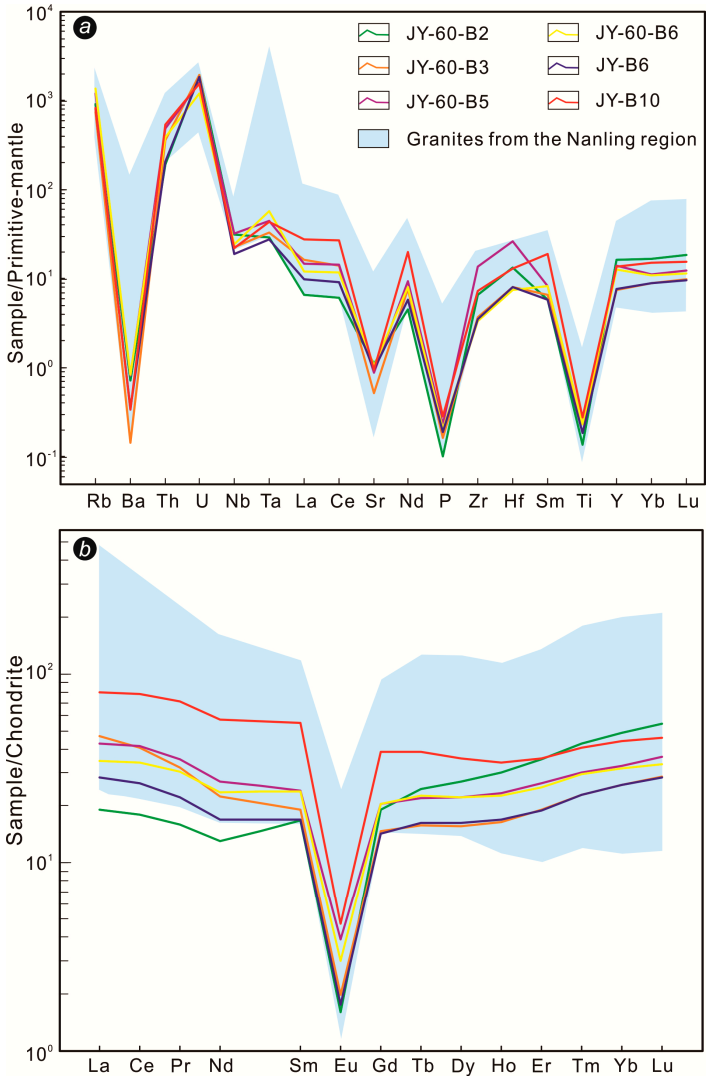

Figure 6. (**a**) Primitive mantle-normalized multiple trace element diagram, the primitive mantle normalization values are from McDonough and Sun. [63]. (**b**) Chondrite-normalized REE pattern diagram, with the chondrite normalization values adopted from Sun and McDonough [64]. Data in the shaded fields for granites in the Nanling area are taken from Zhang et al. [35], Huang et al. [23], Yu et al. [38], Zhou et al. [16], Liu et al. [43] and Gu et al. [25].

4.3. Whole-Rock Sr-Nd-Pb-Hf Isotope Compositions

The whole-rock Sr-Nd-Pb-Hf isotope compositions of the Junye granites are provided in Table 2 with isotopic ratios corrected to 151.9 ± 2.0 Ma (Mei et al., in preparation) based on U-Pb dating of zircons in granite. The granite samples display a range of present-day $^{87}Sr/^{86}Sr$ ratios from 0.844373 to 0.946419 with high $^{87}Rb/^{86}Sr$ ratios of 69.719 to 122.309 and unreasonable initial $^{87}Sr/^{86}Sr$ ratios ranging from 0.680263 to 0.706566. The granites, however, show present-day $^{143}Nd/^{144}Nd$ ratios ranging from 0.512169 to 0.512272 and initial $^{143}Nd/^{144}Nd$ ratios ranging from 0.511988 to 0.512021 that correspond to εNd (152 Ma) values of −8.28 to −8.91 and two-stage depleted mantle model ages (T_{DM2}) of 1645 to 1698 Ma. The age-corrected initial Pb isotopic compositions of the Junye granites are $(^{206}Pb/^{204}Pb)_i$ = 18.646–19.010, $(^{207}Pb/^{204}Pb)_i$ = 15.767–15.786 and $(^{208}Pb/^{204}Pb)_i$ = 39.113–39.159, respectively. Additionally, the samples have $^{176}Lu/^{177}Hf$ of 0.015 to 0.050, $^{176}Yb/^{177}Hf$ of 0.439 to 1.577 and $^{176}Hf/^{177}Hf$ of 0.282507 to 0.282598, respectively, from which initial $^{176}Hf/^{177}Hf$ ratios ranging from 0.282410 to 0.282485 that correspond to εHf(152 Ma) between −6.9 and −9.5 with T_{DM2} ages of 1680 to 2214 Ma are calculated.

Table 2. Bulk rock Sr-Nd-Pb-Hf analyses for Junye granites.

Sample No.	JY-60-B2	JY-60-B3	JY-60-B5	JY-60-B6	JY-B6	JY-B10
Rb(ppm)	578	481	761	860	521	521
Sr(ppm)	23.4	11.1	18.8	22	20	20
$^{87}Sr/^{86}Sr$	0.845472	0.941059	0.946419	0.902160	0.844373	0.863345
±2σ	0.000016	0.000015	0.000018	0.000011	0.000014	0.000012
$^{87}Rb/^{86}Sr$	69.7185	122.3090	114.2518	110.3347	72.4399	73.5265
$(^{87}Sr/^{86}Sr)_i$	0.696814	0.680263	0.702803	0.666897	0.689912	0.706566
Sm(ppm)	2.6	2.9	3.7	3.7	2.6	8.4
Nd(ppm)	6.1	10.5	12.6	11.0	7.92	26.8
$^{143}Nd/^{144}Nd$	0.512272	0.512192	0.512169	0.512222	0.512206	0.512182
±2σ	0.000005	0.000005	0.000005	0.000005	0.000006	0.000005
$^{147}Sm/^{144}Nd$	0.2646	0.1748	0.1836	0.2091	0.2063	0.1965
$(^{143}Nd/^{144}Nd)_i$	0.512013	0.512021	0.511988	0.512016	0.512004	0.511989
εNd(t)[a]	−8.44	−8.28	−8.91	−8.36	−8.61	−8.90
T_{DM2}/Ma	1659	1645	1698	1652	1673	1697
U(ppm)	40.6	40.8	33.4	25.4	38.6	32.7
Th(ppm)	16.2	30.5	41.3	33.5	17.6	46.1
Pb(ppm)	64.4	54.5	62.8	58.3	56.9	49.0
$^{208}Pb/^{204}Pb$	39.280	39.431	39.446	39.432	39.311	39.640
±2σ	0.0021	0.0019	0.0025	0.0020	0.0027	0.0055
$^{207}Pb/^{204}Pb$	15.814	15.842	15.810	15.813	15.827	15.837
±2σ	0.0007	0.0007	0.0008	0.0008	0.0007	0.0013
$^{206}Pb/^{204}Pb$	19.617	20.174	19.614	19.598	19.902	20.039
±2σ	0.0007	0.0008	0.0008	0.0009	0.0008	0.0022
$(208Pb/204Pb)_i$	39.152	39.145	39.113	39.141	39.154	39.159
$(207Pb/204Pb)_i$	15.767	15.785	15.770	15.780	15.776	15.786
$(206Pb/204Pb)_i$	18.646	19.010	18.793	18.926	18.852	19.000
$^{176}Lu/^{177}Hf$	0.015	0.046	0.041	0.032	0.016	0.050
$^{176}Yb/^{177}Hf$	0.439	1.374	1.225	1.000	0.464	1.577
$^{176}Hf/^{177}Hf$	0.282565	0.282524	0.282507	0.282583	0.282598	0.282530
±2σ	0.000003	0.000003	0.000004	0.000004	0.000004	0.000004
$(^{176}Hf/^{177}Hf)_i$	0.282435	0.282410	0.282463	0.282442	0.282485	0.282417
εHf(0)	−7.3	−8.8	−9.4	−6.7	−6.2	−8.6
εHf(t)[b]	−8.6	−9.5	−7.6	−8.4	−6.9	−9.3
T_{DM2}/Ma	1841	2153	1680	1799	2062	2214

a: $T_{DM2} = \ln\{1 + [(^{143}Nd/^{144}Nd)_S - \langle(^{147}Sm/^{144}Nd)_S - (^{147}Sm/^{144}Nd)_C\rangle(e^{\lambda t} - 1) - (^{143}Nd/^{144}Nd)_{DM}]/[(^{147}Sm/^{144}Nd)_C - (^{147}Sm/^{144}Nd)_{DM}]\}/\lambda$; S-sample; C-crust; DM-depleted mantle. b: $T_{DM1} = \{1 + [(^{176}Hf/^{177}Hf)_S - (^{176}Hf/^{177}Hf)_{DM}]/[(^{176}Lu/^{177}Hf)_S - (^{176}Lu/^{177}Hf)_{DM}]\}/\lambda$; $T_{DM2} = T_{DM1} - (T_{DM1} - t)[(f_{CC} - f_S)/(f_{CC} - f_{DM})]$; $f_{Lu/Hf} = (^{176}Lu/^{177}Hf)_s/(^{176}Lu/^{177}Hf)_{CHUR} - 1$; f_{CC}, f_S and f_{DM} is the $f_{Lu/Hf}$ value of the continental crust, sample and depleted mantle, respectively; CHUR is the abbreviation of chondrite uniform reservoir.

5. Discussion

5.1. Genetic Type of Granites

Since the 1970s, the genetic classification system for granitic rocks has gradually become more mature and detailed. Based on the nature of the protolith, they can be generally divided into S-, I-, M- and A-types [21,65–67]. The advantage of this classification is that not only is it capable of indicating the tectonic setting, but it also reflects the characteristics of the magma source. However, it is usually difficult to classify the genetic type of highly evolved granites because the major elements of granitic rocks tend to be the component of the lowest eutectic point after extensive fractional crystallization has occurred, thus making it very difficult to identify protoliths [8,22,23,38].

The data reported in this paper can be used to classify the Junye granites. Firstly, the possibility of Junye granites being of M-type can easily be excluded, because the magmas of M-type granites originate from the mantle and are rich in MgO, Fe_2O_3 and poor in SiO_2 and Al_2O_3 [68], while the

Junye granite samples have high silica, are rich in alkali and low in MgO and Fe_2O_3. In addition, typical S-type granites are commonly characterized by high aluminium saturation indices (ASI > 1.1), relatively low Na_2O (<3.2 wt.%), high P_2O_5 and a positive correlation between ASI and P_2O_5, which are commonly used to distinguish them from I-type granites [21,68,69]. However, the Junye granites have low ASI values ranging from 0.99 to 1.02, relatively high Na_2O (3.48–3.97 wt.%), extremely little P_2O_5 (<0.01 wt.%) and no diagnostic aluminium-rich minerals such as garnet or primary muscovite [8]. Hence, these granites are unlikely to be of S-type.

Previous studies have shown that it is very difficult to distinguish A-type from highly fractionated I-type granites [65,70–73], because these granitic rocks, with increasing degree of differentiation, will simultaneously show the characteristics of A-type and I-type [8,21]. A-type granites are generally enriched in HFSEs (high field strength elements), such as Nb, Zr, Ce, Y and Ga [5], with 10,000 Ga/Al and (Zr + Nb + Ce + Y) being always greater than 2.6 and 350 ppm, respectively [65]. The 10,000 Ga/Al ratios (2.57–2.82, average = 2.67) of the Junye granites, which are similar to those in the Nanling region on the genetic type discrimination diagram, plot in the range of A-type field close to the fields of I- and S-types (Figure 7a,b). This makes it easy to judge these granites as A-type just from the data and diagrams. However, the Ga/Al ratios will gradually increase with increasing degree of magma fractionation or by reworking by hydrothermal fluids at later stages [24,74]. On the diagram of 10,000 Ga/Al vs. Y/Ho (Figure 7d), 10,000 Ga/Al ratios display a rough increase with increasing Y/Ho ratios, which indicates that this is the result of the interaction between fluids and magma [24]. The REE tetrad effects of the Junye granites are consistent with an interpretation of intense interaction between highly evolved magma and volatile-rich (F, Cl, CO_2) hydrothermal fluids [61,62]. In addition, Junye granites have low HFSE contents (the average content 168 ppm of Zr + Ce + Nb + Y is far less than 350 ppm) and have no diagnostic minerals of A-type granite, such as riebeckite, fayalite and aegirine. Thus, the possibility of Junye granites being of A-type can also be ruled out.

Li et al. [8] proposed that most early Yanshanian granitoids in the Nanling region are fractionated I-type granites, which they called typical "Nanling series" granites with the following characteristics: (1) they contain neither amphibole of typical I-type granite nor the diagnostic minerals for S-type granite that mainly include muscovite and garnet; (2) the lithology is dominated by biotite monzogranite and biotite K-feldspar granite with the petrochemical features of high SiO_2 (>73 wt.%), low P_2O_5 (<0.05 wt.%) and metaluminous to peraluminous; (3) zircon U-Pb ages are mainly between 150 and 160 Ma.

Actually, the Junye granitic pluton, which was formed 151.9 ± 2.0 Ma ago, has high SiO_2 and K_2O + Na_2O, low MgO and P_2O_5, and is metaluminous to peraluminous, rich in Rb, Th, U and deficient in Ba, Sr, Ti, P, Eu, thus showing the features of typical "Nanling series" granites. Furthermore, on the Y vs. Rb diagram, the contents of Y raise with the increase in Rb (Figure 7c), displaying the trend of a fractionated I-type granite [8]. Therefore, it can be concluded that, judging from the petrological and geochemical characteristics of the samples, the Junye granites are fractionated I-type granite.

5.2. Magma Source

Previous investigators have proposed three main mechanisms for the formation of I-type granitic magmas, namely (1) partial melting of mafic-intermediate meta-igneous rocks with/without the input of mantle-derived magmatic components [75,76], (2) reworking of sedimentary materials by mantle-like magmas [77,78], and (3) crystal fractionation of basaltic parental magmas [79]. Li et al. [22] proposed that the intermediate to felsic calc-alkaline I-type granitic magmas are commonly derived either from remelting of mafic to intermediate igneous materials, or by fractional crystallization of mantle-like basaltic magmas that are predominantly characterized by higher εHf(t) and εNd(t) values with significant basaltic melt components. However, the Junye granites have negative εNd(t) values ranging from −8.28 to −8.91 with T_{DM2} of 1645–1698 Ma (average = 1671 Ma) (Table 2) and lower εHf(t) values varying from −6.9 to −9.5 with T_{DM2} ages of 1680–2214 Ma (average = 1958 Ma) (Table 2), which collectively indicate a Paleoproterozoic crustal source (Figures 8 and 9c). Thus, the possibility

of Junye granites having been generated by crystal fractionation of mantle-derived basaltic parental magma can be precluded. Moreover, if the granites with Hf T_{DM2} ages around 2.2 Ga (Table 2) (late Paleoproterozoic) were formed by newly mantle-derived magmas reworking sedimentary rocks, any such sedimentary rock should come from older Archean strata in the Nanling region. However, no or very few late Archean rocks have been found in the Cathaysia Block to date [22]. On the other hand, granites generated from reworking of supracrustal materials by mantle-like magmas usually show high A/CNK molar ratios (>1.1) [69] and a wide range of εHf(t) (up to 10 ε unit) [77], such as −9.69 to −0.04 for the Xishan granites in the Guangdong Province [5], −14.2 to 4.8 for the Shaziling granites in the Jiuyishan region [80], −10.4 to 1.4 for the Larong granites in Tibet [81] and −2.9 to 8 for the mafic microgranular enclaves within the −2.9 to 1.6 of Lisong granites in the Nanling region [37]. In comparison, the Junye granites have metaluminous to weakly peraluminous characteristics (molar ratios of A/CNK = 0.97–1.02) (Table 1) and uniform εHf(t) values (−6.9 to −9.5) (Table 2). In fact, such homogeneous and highly negative values of εNd(t) (−8.28 to −8.91) and εHf(t) (−6.9 to −9.5) indicate that there was no input of mafic magma into granitic magma. Hence, the reworking of sedimentary rocks by mantle-derived magmas generating the Junye granites can also be ruled out.

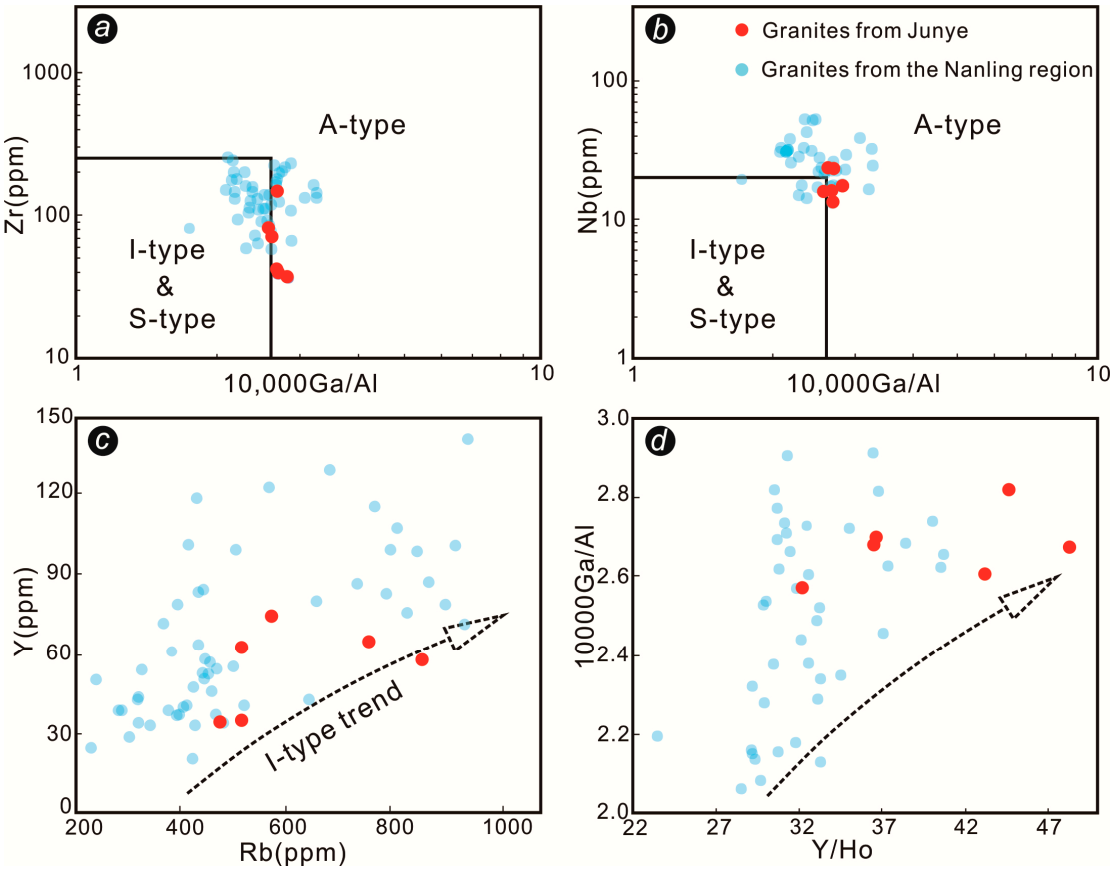

Figure 7. Discrimination diagrams relevant to the genetic type of granites: (**a**,**b**) plots of Zr vs. 10,000 Ga/Al and Nb vs. 10,000 Ga/Al (fields after Whalen et al. [65]); (**c**,**d**) plots of Y vs. Rb and 10,000 Ga/Al vs. Y/Ho. The compositions of trace elements for granites in the Nanling area are cited from Zhang et al. [35], Huang et al. [23], Yu et al. [38], Zhou et al. [16], Liu et al. [43] and Gu et al. [25].

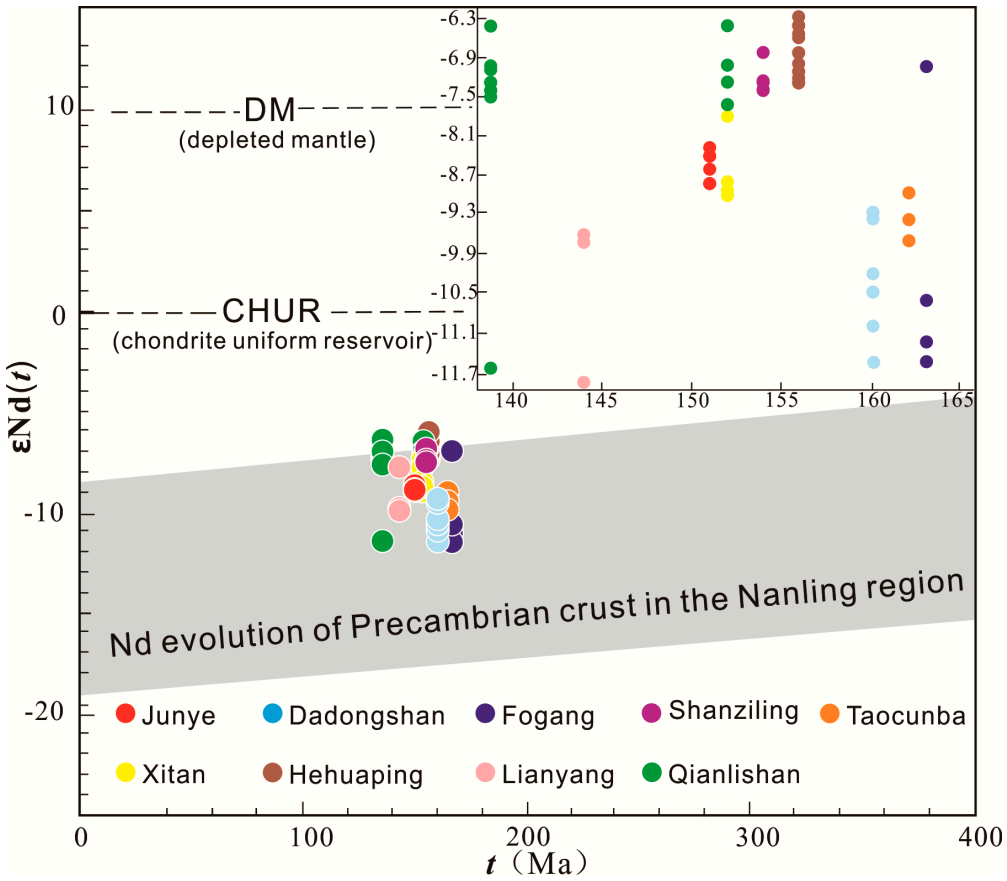

Figure 8. εNd(t) vs. t (Ma) diagram of granites in the Nanling region, modified after Sun et al. [82], showing the ages and εNd(t) values of granite plutons for Junye (this paper), Qianlishan [19], Fogang [26], Dadongshan [23], Xitian [16], Lianyang [83], Taocunba [27], Hehuaping [84] and Shaziling [80].

The Junye granites show a range of unreasonable age-corrected $^{87}Sr/^{86}Sr$ ratios from 0.680263 to 0.706566 with high $^{87}Rb/^{86}Sr$ ratios of 69.7 to 122.3 (Table 2). Obviously, such $(^{87}Sr/^{86}Sr)_i$ values cannot be used for discussing the source of magma, owing to the extensive differentiation of the granitic magma, which resulted in the high Rb/Sr ratios at a late stage [38,85]. However, the homogeneous Nd isotopic compositions with low εNd(t) values (−8.28 to −8.91) are consistent with the coeval granites in the Nanling region, such as the Dadongshan granites (−9.3 to −11.5) [23], Fogang granites (−7.0 to −11.5) [26], Hehuaping granites (−5.1 to −7.3) [84] and Xitian granites (−7.3 to −8.9) [16], which jointly suggest that the granitic magma was derived from Paleoproterozoic crustal materials in the Nanling region (Figure 8). Granite samples all plot in the field of continental magmas and global sediments on the εHf(t) vs. εNd(t) diagram (Figure 9c), suggesting a similar crustal source. The Pb isotopic compositions (Figure 9a,b) cause the Junye samples to plot between upper crust and lower crust, indicating crustal petrogenesis.

On the other hand, there is a sample with $(^{87}Sr/^{86}Sr)_i$ = 0.7066 (Table 2) broadly close to that of magmas derived from partial melting of infracrustal meta-igneous rocks (0.7080) [75], although most of these age-corrected Sr isotopes are untrustworthy. The geochemical traits of low Ni (13.5–24 ppm), Cr (1.7–3.7 ppm) and MgO (0.02–0.04 wt.%) contents similar to those of infracrustal adakitic rocks and meta-basaltic experimental melts [11], pronounced narrow εHf(t) values and low A/CNK [86] show that these granitic magmas are derived from lower crust.

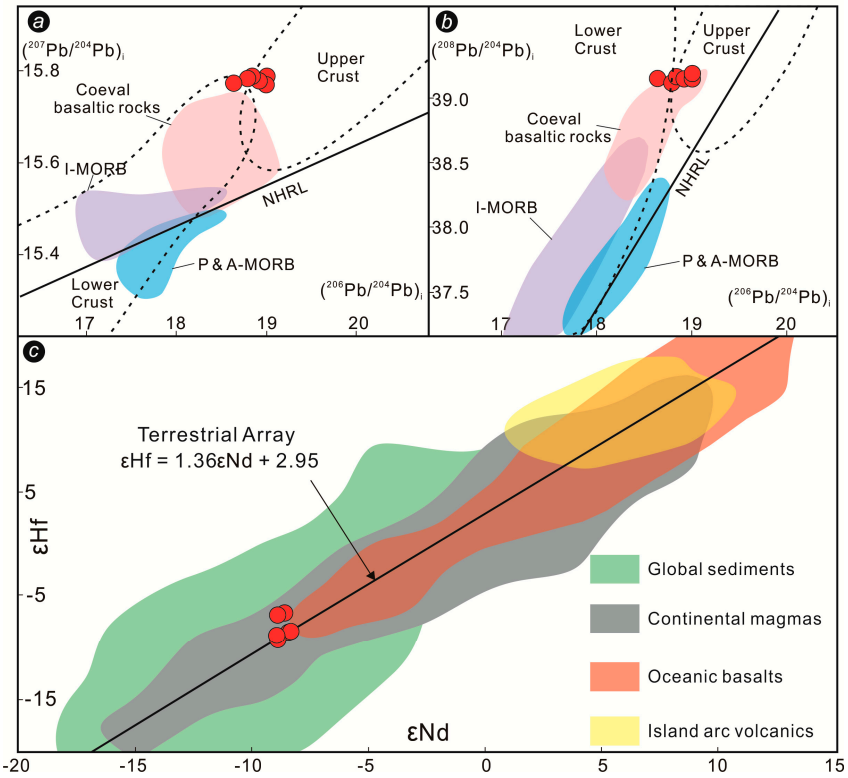

Figure 9. (**a**,**b**) Initial Pb isotopic ratios diagrams of $(^{207}Pb/^{204}Pb)_i$ vs. $(^{206}Pb/^{204}Pb)_i$ and $(^{208}Pb/^{204}Pb)_i$ vs. $(^{206}Pb/^{204}Pb)_i$, modified after Zartman and Doe. [87] and Li et al. [11]. Data source: Northern Hemisphere Reference Line (NHRL) [88], P&A-MORB (Pacific and Atlantic MORB) and I-MORB (Indian MORB) [89] and Pb isotopic compositions of coeval basaltic rocks in the Cathaysia Block [90]. (**c**) Plots of εNd(t) vs. εHf(t) for the Junye pluton, fields after Vervoort et al. [91]; terrestrial array after Vervoort et al. [92].

The Pb isotopes of our granites plot very close to the coeval basaltic rocks formed at 178–150 Ma in South China [90]. The εHf(t)-εNd(t) diagram also would permit an input of oceanic basalts (OIB). However, we believe that these similarities are just fortuitous, because these basaltic rocks mostly have higher εNd(t) varying from −1.7 to 6.6 and younger two-stage Nd model ages, ranging from 0.4 Ga to 1.1 Ga [90], as compared to the Junye granites. The involvement of juvenile mantle-derived magmas in the generation of the Junye granites appears unlikely because the two-stage Nd model ages (1645–1697 Ma) of the Junye granites are basically consistent with the 1700 Ma zircon ages [93] in the basement of the Nanling region, and 1.7 Ga is also considered the peak two-stage Nd model age in the western Cathaysia Block [2]. In fact, the granitic magmas would show more or less mantle-derived isotopic characteristics due to the time elapsed and the process between the separation of a basaltic protolith from mantle and its subsequent partial melting [76]. This is why samples exhibit few isotopic features of coeval basaltic rocks. All evidence in this study leads us to believe that the underplating of these coeval basaltic magmas acted as a heat source to cause melting, rather than the notion that mantle-derived components for the generation of granitic magmas were necessary.

Previous research has suggested that high-K I-type granitic magmas are generally derived from partial melting of calc-alkaline to high-K calc-alkaline, mafic to intermediate meta-igneous rocks in the lower crust [76]. In addition, the melting experiments conducted by Sisson et al. [94] have indicated that high-K melts, with $K_2O/Na_2O > 1$ and $SiO_2 > 65\%$ and mineral assemblages including more plagioclase and Fe-Ti oxide-rich and amphibole-poor, can be produced by the melting of medium- to high-K basaltic rocks at 700 MPa with fO_2 controlled in the range Ni-NiO −1.3 to +4 and temperature between 825 and 925 °C. The characteristics and conditions of these experimental melts were consistent with those of granitic magmas in the Nanling region with the enrichment of plagioclase and biotite,

the absence of amphibole, low Ni, Cr, MgO contents and high SiO_2 and K_2O contents, as well as high magma temperature (>840 °C) [23]. To sum up, we suggest that the Junye highly fractionated I-type granites were probably generated by partial melting of infracrustal medium- to high-K metamorphic basaltic rocks in the Nanling region. This interpretation relies on the following evidence: (1) their geochemical traits of high SiO_2, low MgO, enrichment in LILE, deficiency in HFSE (Table 1), positive Rh, Th, U and negative Nb, Ti, P anomalies (Figure 6a) as well as the initial Nd-Pb-Hf isotopic compositions (Table 2; Figures 8 and 9) are consistent with those of crust-derived magmas [86]; (2) their low Ni, Cr, MgO contents (Table 1) are similar to those of infracrustal adakitic rocks and experimental melts from meta-basaltic rocks [11]; (3) their high SiO_2 and K_2O contents (Table 1) have been observed in medium- to high-K basaltic experimental melts [94]; (4) they have negative and uniform $\varepsilon Nd(t)$ and $\varepsilon Hf(t)$ values as well as the extremely old two stage Nd and Hf model ages (Table 2), suggesting that supracrustal or mantle-like components were not required for the formation of the granitic magmas.

5.3. Fractional Crystallization

There is no doubt that parental magmas underwent strong fractional crystallization during the formation of the Junye granites, as suggested by the high differentiation index (DI = 93.58–94.68) (Table 1) and geochemical characteristics, which include extreme depletion in Ba, Sr, Ti, P and Eu (Figure 6a,b). Moreover, on Harker major elements diagrams, these granites display a systematic correlation between SiO_2 and some major oxides and exhibit an increasing trend of K_2O and decreasing trends of Al_2O_3, CaO, Na_2O, Fe_2O_3 and TiO_2 with increasing SiO_2 (Figure 5), which are also the consequence of fractional crystallization by certain minerals. The SiO_2 content of most granites in the Nanling region have a negative correlation with K_2O (Figure 5c), but a positive correlation with Na_2O (Figure 5d), which generally indicates that the separation of K-feldspar played a relatively important role.

However, contrary to those in the Nanling region, SiO_2 concentrations of the Junye granites correlate positively with K_2O (Figure 5c) and negatively with Na_2O (Figure 5d). Hence, K-feldspar fractional crystallization is not significant, owing to the fact that K_2O contents rise with increasing SiO_2 and coarse-grained K-feldspars are abundant in the Junye high-silica granites. The extremely low contents of Ba (1.01–5.79 ppm) and Sr (11.1–23.4 ppm) (Figure 6a; Table 1) are the result of the separation of biotite and plagioclase, respectively [22]. In addition, the depletions of P and Ti (Figure 6a) suggest the fractionation of apatite and Ti-bearing minerals (such as rutile and ilmenite) [10], respectively, and separation of Fe-Mg-bearing biotite can also result in decreasing contents of MgO and Fe_2O_3 (Figure 5e) during evolution of the granitic magma [22]. The low REE contents are predominantly controlled by the fractionation of accessory minerals, such as apatite, monazite and allanite [21]. However, the anomalies of P, Ti and Sr (Figure 6a) may also be generated by melting process of the infracrustal medium- to high-K metamorphic basaltic rocks. These extreme depletions were also common for the Nanling region with highly evolved magmatism. In fact, REE patterns that display a tetrad effect (Figure 6b) and high $^{87}Rb/^{86}Sr$ ranging from 69.7 to 122.3 (Table 2) also suggest that the parental magmas reflect a highly evolved magmatic system [61,84]. Since almost all samples plot close to the end of the evolution trend lines in the Harker diagrams (Figure 5), the Junye pluton is possibly the product of late-stage granitic magma evolution in the Nanling region. Evidently, these granites, having Zr/Hf ratios of 15.9–20.3 and Y/Ho ratios of 32.2–48.3, do not have CHARAC trace element characteristics ($26 < Zr/Hf < 46$, $24 < Y/Ho < 36$) [95], which indicates the intense interaction between a highly evolved magma and volatile-rich (F, Cl, CO_2) hydrothermal fluids during the late stage of granite formation [61,96].

5.4. Implications for Tectonic Setting and W-Polymetallic Mineralization

Large-scale magmatism is generally considered to be associated with regional tectonic evolution [95]. Such a large-scale granitic magmatism in South China during the Yanshanian period is closely related to its tectonic setting of multi-stage crustal movement [2,3]. Many tectonic models such as the post-orogenic setting [6] and the intraplate extensional or rifting regime [97] have been proposed during past decades. However, it is worth noting that the extensional lithospheric

setting during the emplacement of early Yanshanian granitic magma in the Nanling region was most widely accepted [1,7,13,32]. Different models relevant to subduction of the paleo-Pacific plate have been reported to interpret the large-scale Yanshanian magmatic events in South China. Specifically, the active continental margin model [98,99] could hardly be applied to interpret the widespread magmatic belt (ca. 1300-km-wide) [22]. Meanwhile, the model of changing angles of the subduction of the paleo-Pacific plate beneath southeastern China [100] also cannot explain the occurrence of the Jurassic intra-plate magmatism [22]. Li and Li [1] proposed a flat-subduction model that not only illustrates the broad Indosinian orogen but also accounts for the extensive Mesozoic magmatism. It has been widely accepted to explain the petrogenesis of early Yanshanian granitic magmatism in the Nanling region [12,82,86]. During the middle Jurassic (175–140 Ma), the paleo-Pacific plate migrated inland to South China in the model of NW-trending flat-slab subduction followed by a retreat and foundering of the subducted slab. The subducted oceanic plate fractured and asthenosphere mantle upwelling led directly to large-scale intraplate magmatism in the early Yanshanian period in South China [1,12,30,101]. Large-scale underplating of basaltic magma occurred in the Nanling region during the early Yanshanian period under the tectonic setting of lithospheric extension and thinning, which provided the heat source and/or materials for the granitic magmatism and W-Sn polymetallic mineralization [102]. The high-temperature basaltic magma induced partial melting of the ancient continental crustal rocks in Nanling and its surrounding areas, generating voluminous granitoids [103]. A large number of geochronological data shows that many granitic batholiths with exposed areas larger than 500 km^2 were formed at 165–150 Ma in the Nanling region [22,97].

The granites in the Yiliu region were mostly emplaced at 157–152 Ma. There are no significant negative Nb-Ta anomalies in the granite samples (Figure 6a), which contrasts the characteristics of rocks formed in island arc environments [31]. Like most granitoids in the Nanling region, the Junye samples plot in the fields of within-plate granites (WPG; Figure 10b) and post-orogenic granites (POG; Figure 10a), respectively, indicating these granites were generated by intraplate magmatism during the post-orogenic stage. A continental extensional environment was formed by lithospheric extension and thinning in the Yiliu and its surrounding area under the influence of the flat-slab subduction of the paleo-Pacific plate. The upwelling and underplating of mantle-derived basaltic magma transferred sufficient heat energy to induce partial melting of meta-basaltic rocks in the Paleoproterozoic crust, thus generating the magmatic activity of the intraplate environment and forming the granitic parental magmas. These magmas then experienced strong fractional crystallization during the late stage of magmatic evolution, and were finally emplaced in the Yiliu and its surrounding region.

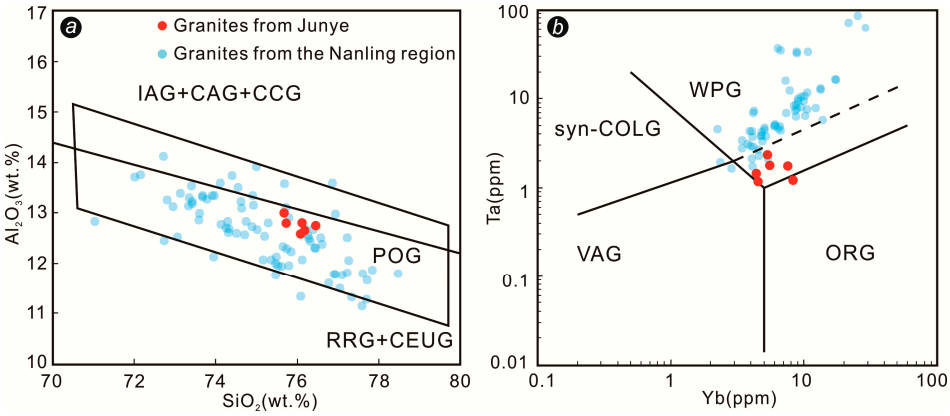

Figure 10. Discrimination diagrams relevant to the tectonic setting: (**a**) plots of Al_2O_3 vs. SiO_2, fields after Maniar et al. [60]; (**b**) plots of Ta vs. Yb, fields after Pearce et al. [104]. Abbreviations: WPG = within plate granites; syn-COLG = syn-collision granites; VAG = volcanic arc granites; ORG = ocean ridge granites; IAG = island arc granites; CAG = continental arc granites; CCG = continental collision granites; POG = post-orogenic granites; RRG = rift related granites; CEUG = continental epeirogenic uplift granites.

During the middle to late Jurassic (165–150 Ma), a large-scale W-Sn polymetallic mineralization event occurred in the Nanling region [32,97]. These W-polymetallic deposits have close temporal and spatial relationships with the coeval granitic magmatism [5,14,15,17]. For example, the granite zircon U-Pb age of 157 ± 1.0 Ma is consistent with the cassiterite U-Pb age of 158 ± 1.9 Ma in the Yaogangxian W-Sn deposit [12], the molybdenite Re-Os age of 154.4 ± 3.8 Ma [105] is similar to the granite U-Pb age of 157.6 ± 3.5 Ma [106] in the Taoxikeng W-polymetallic deposit, and the granite U-Pb age of 151 ± 3.0 Ma [107] is identical to the molybdenite Re-Os age of 151.0 ± 3.5 Ma [108] in the Shizhuyuan W-polymetallic deposit. Judging from the zircon U-Pb age of Junye granites (151.9 ± 2.0 Ma) and Baoshan granites (156.9 ± 2.4 Ma), the timing of metallogenesis for the Yiliu tungsten polymetallic deposit must be consistent with the large-scale W-Sn mineralization in the Nanling region at 165–150 Ma [97], and this time is very likely the same as the emplacement age of the Junye pluton. Additionally, Junye granites are enriched in many ore-forming elements (W, Sn, Pb, Zn, Cu; Table 1), particularly in tungsten (533–781 ppm; Table 1), which is similar to those of coeval granites in the Nanling region. We thus consider that the Yiliu W-polymetallic deposit may be the product of intense interaction between highly evolved granitic magmas at a late stage and volatile-rich ore-forming hydrothermal fluids in the Nanling region, which is supported by the REE tetrad effect patterns (Figure 6b) and Harker diagrams (Figure 5). These granitic magmas possibly provided not only heat but also ore-forming components for the mineralization.

6. Conclusions

(1) Junye biotite monzogranite, emplaced in early Yanshanian and classified as highly fractionated I-type granite, has a high-K calc-alkaline and metaluminous to weakly peraluminous composition. It is enriched in SiO_2 and total alkalis, deficient in P_2O_5, MgO, CaO and $Fe_2O_3{}^T$, and has positive Rb, Th U and negative Ba, Sr, P, Ti anomalies.

(2) The Junye granites are possibly the product of the partial melting of Paleoproterozoic infracrustal medium- to high-K metamorphic basaltic rocks in the Cathaysia Block, caused by the underplating of mantle basaltic magmas that provided abundant heat for melting in a tectonic setting of lithospheric extension and thinning during the late Jurassic period.

(3) The Junye pluton probably underwent intense interaction between highly evolved granitic magmas and volatile-rich hydrothermal fluids at the late stage of formation, and was accompanied by a high degree of fractional crystallization of biotite, plagioclase and accessory minerals, such as apatite, monazite and allanite.

(4) These granitic magmas, with enrichment in W, Sn, Pb, Zn and Cu, possibly provide not only a heat source but also ore-forming materials for the regional W-polymetallic mineralization.

Author Contributions: T.W., Z.H. and M.Y. proposed and organized the project and designed the experiment. T.W. interpreted the data and wrote the main manuscript. Z.H., D.Z., J.Z. and C.W. revised the main manuscript. All the authors discussed the study. All authors have read and agreed to the published version of the manuscript.

Funding: This research was funded jointly by the Science and Technology Support Project of Guizhou Province, China (No. [2019]2859) and the Geological Survey Project of China Geological Survey Bureau (No. [2014]04-025-043).

Acknowledgments: We thank Neng-Ping Shen and Jian-Xing Zhao for the help with trace elements and Sr-Nd-Pb-Hf isotopes analyses. We are also indebted to the Nonferrous Metals Geological Bureau of the Guangdong Province for their permission to investigate and sample the Junye Pluton. We are grateful to two anonymous reviewers for the thoughtful comments. Their constructive and stimulating suggestions helped to significantly improve the manuscript.

Conflicts of Interest: The authors declare no conflict of interest.

References

1. Li, Z.X.; Li, X.H. Formation of the 1300-km-wide intracontinental orogen and postorogenic magmatic Province in Mesozoic South China: A flat-slab subduction model. *Geology* **2007**, *35*, 179–182. [CrossRef]

2. Xu, X.S.; O'Reilly, S.Y.; Griffin, W.L.; Wang, X.L.; Pearson, N.J.; He, Z.Y. The crust of Cathaysia: Age, Assembly and reworking of two terranes. *Precambrian Res.* **2007**, *158*, 51–78. [CrossRef]
3. Charvet, J.; Shu, L.S.; Faure, M.; Choulet, F.; Wang, B.; Lu, H.F.; Breton, N.L. Structural development of the Lower Paleozoic belt of South China: Genesis of an intracontinental orogen. *J. Asian Earth Sci.* **2010**, *39*, 309–330. [CrossRef]
4. Wang, Y.J.; Fan, W.M.; Zhang, G.W.; Zhang, Y.H. Phanerozoic tectonics of the South China Block: Key observations and controversies. *Gondwana Res.* **2013**, *23*, 1273–1305. [CrossRef]
5. Zheng, W.; Mao, J.W.; Zhao, H.J.; Ouyang, H.G.; Zhao, C.S.; Yu, X.F. Geochemistry, Sr-Nd-Pb-Hf isotopes systematics and geochronological constrains on petrogenesis of the Xishan A-type granite and associated W-Sn mineralization in Guangdong Province, South China. *Ore Geol. Rev.* **2017**, *88*, 739–752. [CrossRef]
6. Chen, P.R.; Hua, R.M.; Zhang, B.D.; Lu, J.J.; Fan, C.F. Early Yanshanian postorogenic granitoids in the Nanling region: Petrological constraints and geodynamic settings. *Sci. China* **2002**, *45*, 755–768.
7. Li, X.H.; Chen, Z.G.; Liu, D.Y.; Li, W.X. Jurassic gabbro-granite-syenite suites from southern Jiangxi Province, SE China: Age, origin, and tectonic significance. *Int. Geol. Rev.* **2003**, *45*, 898–921. [CrossRef]
8. Li, X.H.; Li, W.X.; Li, Z.X. On the genetic classification and tectonic implications of the Early Yanshanian granitoids in the Nanling Range, South China. *Chin. Sci. Bull* **2007**, *52*, 1873–1885. [CrossRef]
9. Huang, H.Q.; Li, X.H.; Li, W.X.; Li, Z.X. Formation of high $\delta^{18}O$ fayalite-bearing A-type granite by high-temperature melting of granulitic metasedimentary rocks, southern China. *Geology* **2011**, *39*, 903–906. [CrossRef]
10. Xia, Y.; Xu, X.S.; Zou, B.; Liu, L. Early Paleozoic crust-mantle interaction and lithosphere delamination in South China Block: Evidence from geochronology, geochemistry, and Sr-Nd-Hf isotopes of granites. *Lithos* **2014**, *184*, 416–435. [CrossRef]
11. Li, B.; Jiang, S.Y.; Zhang, Q.; Zhao, H.X.; Zhao, K.D. Geochemistry, geochronology and Sr-Nd-Pb-Hf isotopic compositions of Middle to Late Jurassic syenite-granodiorites-dacite in South China: Petrogenesis and tectonic implications. *Gondwana Res.* **2016**, *35*, 217–237. [CrossRef]
12. Li, W.S.; Ni, P.; Wang, G.G.; Yang, Y.L.; Pan, J.Y.; Wang, X.L.; Chen, L.L.; Fan, M.S. A possible linkage between highly fractionated granitoids and associated W-mineralization in the Mesozoic Yaogangxian granitic intrusion, Nanling region, South China. *J. Asian Earth Sci.* **2020**, *193*, 1–18. [CrossRef]
13. Hua, R.M.; Chen, P.R.; Zhang, W.L.; Yao, J.M.; Lin, J.F.; Zhang, Z.S.; Gu, S.Y.; Liu, X.D.; Qi, H.W. Metallogenesis related to Mesozoic granitoids in the Nanling Range, South China and their geodynamic settings. *Acta Geol. Sin.* **2005**, *79*, 810–820.
14. Jiang, S.Y.; Zhao, K.D.; Jiang, Y.H.; Ling, H.F.; Ni, P. New type of tin mineralization related to granite in South China: Evidence from mineral chemistry, element and isotope geochemistry. *Acta Petrol. Sin.* **2006**, *22*, 2509–2516. (In Chinese with English abstract)
15. Peng, J.T.; Zhou, M.F.; Hu, R.Z.; Shen, N.P.; Yuan, S.D.; Bi, X.W.; Du, A.D.; Qu, W.J. Precise molybdenite Re-Os and mica Ar-Ar dating of the Mesozoic Yaogangxian tungsten deposit, central Nanling district, south China. *Miner. Depos.* **2006**, *41*, 661–669. [CrossRef]
16. Zhou, Y.; Liang, X.R.; Liang, X.Q.; Wu, S.C.; Jiang, Y.; Wen, S.N.; Cai, Y.F. Geochronology and geochemical characteristics of the Xitian Tungsten-Tin- Bearing A-type granites, Hunan Province, China. *Geotecton. Metallog.* **2013**, *37*, 511–529. (In Chinese with English abstract)
17. Zhang, S.G.; Yuan, Y.; Yao, C.X. Petrology and ore-control of Zhuguangshan composite granitic pluton in middle section of Nanling region. *Chin. J. Nonferrous Met.* **2014**, *24*, 1585–1598. (In Chinese with English abstract)
18. Yuan, Y.B.; Yuan, S.D.; Mao, J.W.; Zhao, P.L.; Yan, C.; Zhao, H.J.; Zhang, D.L.; Shuang, Y.; Peng, J.T. Recognition of Late Jurassic W-Sn mineralization and its exploration potential on the western margin of the Caledonian Guidong granite batholith, Nanling Range, South China: Geochronological evidence from the Liuyuan Sn and Zhuyuanli W deposits. *Ore Geol. Rev.* **2018**, *93*, 200–210. [CrossRef]
19. Mao, J.W.; Li, Y.H.; Pei, R.F. Nd-Sr isotopic and petrogenetic studies of the Qianlishan granite stock, Hunan Province. *Miner. Depos.* **1995**, *14*, 235–242. (In Chinese with English abstract)
20. Chen, J.F.; Jahn, B. Crustal evolution of southeastern China: Nd and Sr isotopic evidence. *Tectonophysics* **1998**, *284*, 101–133. [CrossRef]
21. Wu, F.Y.; Jahn, B.M.; Wilde, S.A.; Lo, C.H.; Yui, T.F.; Lin, Q.; Ge, W.C.; Sun, D.Y. Highly fractionated I-type granites in NE China (I): Geochronology and petrogenesis. *Lithos* **2003**, *66*, 241–273. [CrossRef]

22. Li, X.H.; Li, Z.X.; Li, W.X.; Liu, Y.; Yuan, C.; Wei, G.J.; Qi, C.S. U-Pb zircon, geochemical and Sr-Nd-Hf isotopic constraints on age and origin of Jurassic I- and A-type granites from central Guangdong, SE China: A major igneous event in response to foundering of a subducted flat-slab? *Lithos* **2007**, *96*, 186–204. [CrossRef]
23. Huang, H.Q.; Li, X.H.; Li, W.X.; Liu, Y. Age and Origin of the Dadongshan Granite from the Nanling Range: SHRIMP U-Pb Zircon Age, Geochemistry and Sr-Nd-Hf Isotopes. *Geol. J. China Univ.* **2008**, *14*, 317–333. (In Chinese with English abstract)
24. Chen, J.Y.; Yang, J.H. Petrogenesis of the Fogang highly fractionated I-type granitoids: Constraints from Nb, Ta, Zr and Hf. *Acta Petrol. Sin.* **2015**, *31*, 846–854.
25. Gu, R.Q.; Chen, Y.R.; Li, R.J.; Jiang, X.; Li, J.C.; Bai, Y.H.; Nong, Y.J.; Wang, Z.Y.; Yan, X. Comparison of geochemical characteristics of the main granites in Huashan and Guposhan, Guangxi. *Miner. Resour. Geol.* **2019**, *33*, 690–697. (In Chinese with English abstract)
26. Liu, C.S.; Chen, X.M.; Wang, R.C.; Zhang, A.C.; Hu, H. The products of partial melting of the lower crust origin of Early Yanshanian Lapu monzogranite, Guangdong Province. *Geol. J. China Univ.* **2005**, *11*, 343–357. (In Chinese with English abstract)
27. Shan, Z.B.; Li, K.; Ling, H.F.; Shen, W.Z.; Huang, G.L.; Zhu, B. Zircon U-Pb geochronology, geochemistry and petrogenesis of the Taocunba granite, northern Guangdong Province. *Geol. J. China Univ.* **2014**, *20*, 341–352. (In Chinese with English abstract)
28. Wang, X.; Ren, M.H. Constraints of hydrothermal and magmatic zircon on the origin of the Yaogangxian tungsten deposit, Southern China. *Ore Geol. Rev.* **2018**, *101*, 453–467. [CrossRef]
29. Li, X.H. Cretaceous magmatism and lithospheric extension in Southeast China. *J. Asian Earth Sci.* **2000**, *18*, 293–305. [CrossRef]
30. Li, X.H.; Chung, S.L.; Zhou, H.W.; Lo, C.H.; Liu, Y.; Chen, C.H. Jurassic intraplate magmatism in Southern Hunan-Eastern Guangxi: $^{40}Ar/^{39}Ar$ dating, geochemistry, Sr-Nd isotopes and implications for the tectonic evolution of SE China. *Geol. Soc. Lond. Spec. Publicat.* **2004**, *26*, 193–215. [CrossRef]
31. Zhou, X.M.; Sun, T.; Shen, W.Z.; Shu, L.S.; Niu, Y.L. Petrogenesis of Mesozoic granitoids and volcanic rocks in South China: A response to tectonic evolution. *Episodes* **2006**, *29*, 26–33. [CrossRef] [PubMed]
32. Mao, J.W.; Cheng, Y.B.; Chen, M.H.; Pirajno, F. Major types and time-space distribution of Mesozoic ore deposits in South China and their geodynamic settings. *Miner. Deposita* **2013**, *48*, 267–294.
33. Chen, X.M.; Wang, R.C.; Liu, C.S.; Hu, H.; Zhang, W.L.; Gao, J.F. Isotopic dating and genesis for Fogang biotite granite of Conghua area, Guangdong Province. *Geol. J. China Univ.* **2002**, *8*, 293–307. (In Chinese with English abstract)
34. Bao, Z.W.; Zhao, Z.H. Geochemistry and tectonic setting of the Fogang aluminous A-type granite, Guangdong Province, China—A Preliminary study. *Geol. Geochem.* **2003**, *31*, 52–61. (In Chinese with English abstract)
35. Zhang, M.; Chen, P.R.; Zhang, W.R.; Chen, W.F.; Li, H.M.; Zhang, M.Q. Geochemical characteristics and petrogenesis of Dadongshan granite pluton in Nanling Range. *Geochimica* **2003**, *32*, 529–539. (In Chinese with English abstract)
36. Zhao, K.D.; Jiang, S.Y.; Jiang, Y.H.; Liu, D.Y. SHRIMP U-Pb dating of the Furong unite of Qitianling granite from southestern Hunan Province and their geological implications. *Acta Petrol. Sin.* **2006**, *22*, 2611–2616.
37. Li, X.H.; Li, W.X.; Wang, X.C.; Li, Q.L.; Liu, Y.; Tang, G.Q. Role of mantle-derived magma in genesis of early Yanshanian granites in the Nanling range, south China: In situ zircon Hf-O isotopic constraints. *Sci. China Ser. D Earth Sci.* **2009**, *52*, 1262–1278. [CrossRef]
38. Yu, C.F.; Zhao, H.J.; Chen, M.H.; Luo, D.L.; Guo, M.; Wang, Z.H. Geochemical features and petrogenesis of the Dajinshan granites in west Guangdong Province. *Geol. China* **2012**, *39*, 1670–1689. (In Chinese with English abstract)
39. Pei, T.C. Preliminary analysis to metallotects and minerogenetic regularity of endogenic metal mineral resource in Shaoguan-Ruyuan area. *Miner. Resour. Geol.* **1990**, *4*, 1–10. (In Chinese with English abstract)
40. Tang, Y.A.; Lai, J.Q.; Yang, M.; Mei, J.J.; Liu, Q.; Wu, J.; Chen, H.C.; Guo, L.X.; Hu, L.F.; He, Q.J. Characteristics of fluid inclusions of the Yiliu tungsten deposit in Shaoguan, Guangdong Province and implications for metallogenesis. *Acta Geol. Sin.* **2017**, *91*, 2240–2255. (In Chinese with English abstract)
41. Tang, Y.A.; Lai, J.Q.; Yang, M.; Mei, J.J.; Wu, J.; Chen, H.C.; Guo, L.X. Characteristics of fluid inclusions and metallogenesis of Meizichong Pb-Zn-W polymetallic deposit in Guangdong Province. *Geol. Explor.* **2017**, *53*, 217–226. (In Chinese with English abstract)

42. Mei, J.J.; Lai, J.Q.; Tang, Y.A. Study on metallogenic regularity of Ruyuan Yiliu orefield, Guangdong Province. *Acta Mineral. Sin.* **2015**, *S1*, 50. (In Chinese)
43. Liu, Q.; Lai, J.Q. Genesis and tectonic environment of Baoshan pluton in Ruyuan, Guangdong. *Land Resour. Her.* **2016**, *13*, 14–20. (In Chinese with English abstract)
44. Zhou, M.F.; Yan, D.P.; Kennedy, A.K.; Li, Y.Q.; Ding, J. SHRIMP U-Pb zircon geochronological and geochemical evidence for Neoproterozoic arc-magmatism along the western margin of the Yangtze Block, South China. *Earth Planet Sci. Lett.* **2002**, *196*, 51–67. [CrossRef]
45. Zheng, Y.F.; Wu, R.X.; Wu, Y.B.; Zhang, S.B.; Yuan, H.; Wu, F.Y. Rift melting of juvenile arc-derived crust: Geochemical evidence from Neoproterozoic volcanic and granitic rocks in the Jiangnan Orogen, South China. *Precambr. Res.* **2008**, *163*, 351–383. [CrossRef]
46. Charvet, J. The Neoproterozoic-Early Paleozoic tectonic evolution of the South China Block: An overview. *J. Asian Earth Sci.* **2013**, *74*, 198–209. [CrossRef]
47. Shu, L.S.; Zhou, X.M.; Deng, P.; Yu, X.Q. Principal Geological Features of Nanling Tectonic Belt, South China. *Geol. Rev.* **2006**, *52*, 251–265. (In Chinese with English abstract)
48. Wang, X.L.; Zhao, G.C.; Zhou, J.C.; Liu, Y.S.; Hu, J. Geochronology and Hf isotopes of zircon from volcanic rocks of the Shuangqiaoshan Group, South China: Implications for the Neoproterozoic tectonic evolution of the eastern Jiangnan orogen. *Gondwana Res.* **2008**, *14*, 355–367. [CrossRef]
49. Yao, J.L.; Shu, L.S.; Santosh, M. Detrital zircon U-Pb geochronology, Hf- isotopes and geochemistry-new clues for the Precambrian crustal evolution of Cathaysia Block, South China. *Gondwana Res.* **2011**, *20*, 553–567. [CrossRef]
50. Zhu, J.C.; Chen, J.; Wang, R.C.; Lu, J.J.; Xie, L. Early Yanshanian NE trending Sn/W bearing A-type granites in the western-middle part of Nanling Mts region. *Geol. J. China Univ.* **2008**, *14*, 474–484. (In Chinese with English abstract)
51. Kamber, B.S.; Greig, A.; Schoenberg, R.; Collerson, K.D. A refined solution to Earth's hidden niobium: Implications for evolution of continental crust and mode of core formation. *Precambrian Res.* **2003**, *126*, 289–308. [CrossRef]
52. Eggins, S.M.; Woodhead, J.D.; Kinsley, L.P.J.; Mortimer, G.E.; Sylvester, P.; McCulloch, M.T.; Hergt, J.M.; Handler, M.R. A simple method for the precise determination of ≥ 40 trace elements in geological samples by ICP-MS using enriched isotope internal standardisation. *Chem. Geol.* **1997**, *134*, 311–326. [CrossRef]
53. Li, B.P.; Greig, A.; Zhao, J.X.; Collerson, K.D.; Quan, K.S.; Meng, Y.H.; Ma, Z.L. ICP-MS trace element analysis of Song dynasty porcelains from Ding, Jiexiu and Guantai kilns, north China. *J. Archaeol. Sci.* **2005**, *32*, 251–259. [CrossRef]
54. Pin, C.; Francisco, J.C.; Zaldueguil, S. Sequential separation of light rare-earth elements, thorium and uranium by miniaturized extraction chromatography: Application to isotopic analyses of silicate rocks. *Anal. Chim. Acta* **1997**, *339*, 79–89. [CrossRef]
55. Deniel, C.; Pin, C. Single-stage method for the simultaneous isolation of lead and strontium from silicate samples for isotopic measurements. *Anal. Chim. Acta* **2001**, *426*, 95–103. [CrossRef]
56. Mikova, J.; Denkova, P. Modified chromatographic separation scheme for Sr and Nd isotope analysis in geological silicate samples. *J. Geosci.* **2007**, *52*, 221–226.
57. Middlemost, E.A.K. Naming materials in the magma/igneous rock system. *Earth Sci. Rev.* **1994**, *37*, 215–224. [CrossRef]
58. Sylvester, P.J. Post-collisional alkaline granites. *J. Geol.* **1989**, *97*, 261–280. [CrossRef]
59. Peccerillo, R.; Taylor, S.R. Geochemistry of Eocene calc-alkaline volcanic rocks from the Kastamonu area, Northern Turkey. *Contrib. Mineral. Petrol.* **1976**, *58*, 63–81. [CrossRef]
60. Maniar, P.D.; Piccoli, P.M. Tectonic discrimination of granitoids. *Geol. Soc. Am. Bull.* **1989**, *101*, 635–643. [CrossRef]
61. Jahn, B.; Wu, F.Y.; Capdevila, R.; Martineau, F.; Zhao, Z.H.; Wang, Y.X. Highly evolved juvenile granites with tetrad REE patterns: The Woduhe and Baerzhe granites from the Great Xing'an Mountains in NE China. *Lithos* **2001**, *59*, 171–198. [CrossRef]
62. Zhao, Z.H.; Bao, Z.W.; Qiao, Y.L. A peculiar composite M- and W-type REE tetrad effect: Evidence from the Shuiquangou alkaline syenite complex, Hebei Province, China. *Chin. Sci. Bull.* **2010**, *55*, 2685–2696. [CrossRef]
63. McDonough, W.F.; Sun, S.S. The composition of the Earth. *Cheml. Geol.* **1995**, *120*, 223–253. [CrossRef]

64. Sun, S.S.; McDonough, W.F. Chemical and isotopic systematics of oceanic basalts: Implications for mantle composition and processes. *Geol. Soci. Spec. Pub.* **1989**, *42*, 313–345. [CrossRef]
65. Whalen, J.B.; Currie, K.L.; Chappell, B.W. A-type granites: Geochemical characteristics, discrimination and petrogenesis. *Contrib. Mineral. Petrol.* **1987**, *95*, 407–419. [CrossRef]
66. Chappell, B.W.; White, A.J.R. Two contrasting granite types: 25 years later. *Aust. J. Earth Sci.* **2001**, *48*, 489–499. [CrossRef]
67. Bonin, B. A-type granites and related rocks: Evolution of a concept, problems and prospects. *Lithos* **2007**, *97*, 1–29. [CrossRef]
68. Chappell, B.W.; Whilte, A.J.R. Two contrasting granite types. *Pac. Geol.* **1974**, *8*, 173–174.
69. Chappell, B.W. Aluminium saturation in I- and S-type granites and the characterization of fractionated haplogranites. *Lithos* **1999**, *46*, 535–551. [CrossRef]
70. Landenberger, B.; Collins, W.J. Derivation of A-type granites from a dehydrated charnockitic lower crust: Evidence from the Chaelundi complex, eastern Australia. *J. Petrol.* **1996**, *37*, 145–170. [CrossRef]
71. King, P.L.; Chappell, B.W.; Allen, C.M.; White, A.J.R. Are A-type granites the high-temperature felsic granites? Evidence from fractionated granites of the Wangrah Suite. *Aust. J. Earth Sci.* **2001**, *48*, 501–514. [CrossRef]
72. Zhao, J.L.; Qiu, J.S.; Liu, L.; Wang, R.Q. The Late Cretaceous I-and A-type granite association of southeast China: Implications for the origin and evolution of postcollisional extensional magmatism. *Lithos* **2016**, *240*, 16–33. [CrossRef]
73. Guo, X.Z.; Jia, Q.Z.; Lü, X.B.; Li, J.C.; Kong, H.L.; Yao, X.G. The Permian Sn metallogenic event and its geodynamic setting in East Kunlun, NW China: Evidence from zircon and cassiterite geochronology, geochemistry, and Sr-Nd-Hf isotopes of the Xiaowolong skarn Sn deposit. *Ore Geol. Rev.* **2020**, *118*, 1–15. [CrossRef]
74. Eby, G.N. Chemical subdivision of the A-type granitoids: Petrogenetic and tectonic implications. *Geology* **1992**, *20*, 641–644. [CrossRef]
75. Chappell, B.; Stephens, W. Origin of infracrustal (I-type) granite magmas. *Earth Environ. Sci. Trans. R. Soc. Edinb.* **1988**, *79*, 71–86. [CrossRef]
76. Roberts, M.P.; Clemens, J.D. Origin of high-potassium, talc-alkaline, I-type granitoids. *Geology* **1993**, *21*, 825–828. [CrossRef]
77. Kemp, A.I.S.; Hawkesworth, C.J.; Foster, G.L.; Paterson, B.A.; Woodhead, J.D.; Hergt, J.M.; Gray, C.M.; Whitehouse, M.J. Magmatic and crustal differentiation history of granitic rocks from Hf-O isotopes in zircon. *Science* **2007**, *315*, 980–983. [CrossRef]
78. Huang, H.Q.; Li, X.H.; Li, Z.X.; Li, W.X. Intraplate crustal remelting as the genesis of Jurassic high-K granites in the coastal region of the Guangdong Province, SE China. *J. Asian Earth Sci.* **2013**, *74*, 280–302. [CrossRef]
79. Macpherson, C.G.; Dreher, S.T.; Thirlwall, M.F. Adakites without slab melting: High pressure differentiation of island arc magma, Mindanao, the Philippines. *Earth Planet. Sci. Lett.* **2006**, *243*, 581–593. [CrossRef]
80. Li, J.F.; Fu, J.M.; Ma, C.Q.; Lu, Y.Y.; Cheng, S.B.; Ma, L.Y.; Qin, Z.W. Petrogenesis and tectonic setting of the Shaziling pluton in Jiuyishan Area, Nanling: Evidence from Zircon U-Pb geochronology, petrogeochemistry, and Sr-Nd-Hf isotopes. *Earth Sci.* **2020**, *45*, 375–388. (In Chinese with English abstract)
81. Liu, J.; Li, W.C.; Zhu, X.P.; Wang, B.D.; Jiang, J.S.; Liu, H.F. Magmatic evolution and related W–Mo mineralization in the Larong deposit, eastern Tibet: Evidence from zircon U-Pb ages, geochemistry and Sr-Nd-Hf isotopes. *Ore Geol. Rev.* **2020**, *120*, 1–28. [CrossRef]
82. Sun, T.; Zhou, X.M.; Chen, P.R.; Li, H.M.; Zhou, H.Y.; Wang, Z.C.; Shen, W.Z. Strongly peraluminous granites of Mesozoic in Eastern Nanling Range, Southern China: Petrogenesis and implications for tectonics. *Sci. China Ser. D Earth Sci.* **2005**, *48*, 165–174. [CrossRef]
83. Ma, X.H.; Chen, B.; Wang, Z.Q.; Gao, L.; Sun, K.K. Petrogenesis of the Lianyang composite granite, Nanling region: U-Pb zircon geochronology, geochemistry and Nd-Hf isotopes constraints. *Front. Earth Sci.* **2014**, *21*, 264–280. (In Chinese with English abstract)
84. Zhang, R.Q.; Lu, J.J.; Wang, R.C.; Yao, Y.; Ding, D.; Hu, J.B.; Zhang, H.F. Petrogenesis of W- and Sn-bearing granites and the mechanism of their metallogenic diversity in the Wangxianling area, southern Hunan Province. *Geochimica* **2016**, *45*, 105–132. (In Chinese with English abstract)
85. Wu, F.Y.; Sun, D.Y.; Li, H.M.; Jahn, B.M.; Wilde, S. A-type granites in northeastern China: Age and geochemical constraints on their petrogenesis. *Chem. Geol.* **2001**, *187*, 143–173. [CrossRef]

86. Cao, H.W.; Zhang, Y.H.; Santosh, M.; Li, G.M.; Hollis, S.P.; Zhang, L.K.; Pei, Q.M.; Tang, L.; Duan, Z.M. Petrogenesis and metallogenic implications of Cretaceous magmatism in Central Lhasa, Tibetan Plateau: A case study from the Lunggar Fe skarn deposit and perspective review. *J. Geol.* **2019**, *54*, 2323–2346. [CrossRef]
87. Zartman, R.E.; Doe, B.R. Plumbotectonics—The model. *Tectonophysics* **1981**, *75*, 135–162. [CrossRef]
88. Hart, S.R. A large-scale isotope anomaly in the southern hemisphere mantle. *Nature* **1984**, *309*, 753–757. [CrossRef]
89. Hofmann, A.W. Sampling mantle heterogeneity through oceanic basalts: Isotopes and trace elements. *Mantle Core* **2003**, *2*, 61–101.
90. Wang, Y.J.; Fan, W.M.; Cawood, P.A.; Li, S.Z. Sr-Nd-Pb isotopic constraints on multiple mantle domains for Mesozoicmafic rocks beneath the South China Block hinterland. *Lithos* **2008**, *106*, 297–308. [CrossRef]
91. Vervoort, J.D.; Blichert-Toft, J.; Patchett, P.J.; Albarède, F. Relationships between Lu-Hf and Sm-Nd isotopic systems in the global sedimentary system. *Earth Planet. Sci. Lett.* **1999**, *168*, 79–99. [CrossRef]
92. Vervoort, J.D.; Plank, T.; Prytulak, J. The Hf-Nd isotopic composition of marine sediments. *Geochim. Cosmochim. Acta* **2011**, *75*, 5903–5926. [CrossRef]
93. Gao, J.F.; Ling, H.F.; Sheng, W.Z.; Lu, J.J.; Zhang, M.; Huang, G.L.; Tan, Z.Z. Geochemistry and petrogenesis of Lianyang granite composite, west Guangdong Province. *Acta Petrol. Sin.* **2005**, *21*, 1645–1656. (In Chinese with English abstract)
94. Sisson, T.W.; Ratajeski, K.; Hankins, W.B.; Glazner, A.F. Voluminous granitic magmas from common basaltic sources. *Contrib. Mineral. Petrol.* **2005**, *148*, 635–661. [CrossRef]
95. Bau, M. Controls on the fractionation of isovalent trace elements in magmatic and aqueous systems: Evidence from Y/Ho, Zr/Hf, and lanthanide tetrad effect. *Contrib. Mineral. Petrol.* **1996**, *123*, 323–333. [CrossRef]
96. Pitcher, W.S.; Bussell, M.A. Structural control of batholithic emplacement in Peru: A review. *J. Geol. Soc.* **1997**, *133*, 249–255. [CrossRef]
97. Mao, J.W.; Xie, G.Q.; Guo, C.L.; Chen, Y.C. Large-scale tungsten-tin mineralization in the Nanling region, South China: Metallogenic ages and corresponding geodynamic process. *Acta Petrol. Sin.* **2007**, *23*, 2329–2338. (In Chinese with English abstract)
98. Martin, H.; Bonin, B.; Capdevila, R.; Jahn, B.M.; Lameyre, J.; Wang, Y. The Kuiqi peralkaline granitic complex (SE China): Petrology and geochemistry. *J. Petrol.* **1994**, *35*, 983–1015. [CrossRef]
99. Lan, C.Y.; Jahn, B.M.; Mertzman, S.A.; Wu, T.W. Subduction-related granitic rocks of Taiwan. *J. Southeast Asian Earth Sci.* **1996**, *14*, 11–28. [CrossRef]
100. Zhou, X.M.; Li, W.X. Origin of the Late Mesozoic igneous rocks in Southeastern China: Implications for lithosphere subduction and underplating of mafic magmas. *Tectonophysics* **2000**, *326*, 269–287. [CrossRef]
101. Zhou, Z.M.; Ma, C.Q.; Wang, L.X. A source-depleted Early Jurassic granitic pluton from South China: Implication to the Mesozoic Juvenile accretion of the South China crust. *Lithos* **2018**, *300–301*, 278–290. [CrossRef]
102. Mao, J.W.; Xie, G.Q.; Li, X.F. Mesozoic large scale mineralization and multiple lithospheric extension in South China. *Earth Sci. Front.* **2004**, *11*, 45–55. (In Chinese with English abstract)
103. Hua, R.M.; Chen, P.R.; Zhang, W.L.; Yao, J.M.; Lin, J.F.; Zhang, Z.S.; Gu, S.Y. Metallogenesis and their geodynamic settings related to Mesozoic granitoids in the Nanling range. *Geol. J. China Univ.* **2009**, *11*, 291–304. (In Chinese with English abstract)
104. Pearce, J.A.; Harris, N.B.W.; Tindle, A.G. Trace element discrimination diagrams for the tectonic interpretation of granitic rocks. *J. Petrol.* **1984**, *25*, 956–983. [CrossRef]
105. Chen, Z.H.; Wang, D.H.; Qu, W.J.; Chen, Y.C.; Wang, P.A.; Xu, J.X.; Zhang, J.J.; Xu, M.L. Geological characteristics and mineralization age of the Taoxikeng tungsten deposit in Chongyi County, southern Jiangxi Province, China. *Geol. Bull. China* **2006**, *25*, 496–501. (In Chinese with English abstract)
106. Guo, C.L.; Wang, D.H.; Chen, Y.C.; Wang, Y.B.; Chen, Z.H.; Liu, S.B. Precise SHRIMP zircon U-Pb and quartz vein Rb-Sr dating of the Mesozoic Taoxikeng tungsten polymetallic deposit, eastern Nanling district, South China. *Miner. Depos.* **2007**, *26*, 432–442. (In Chinese with English abstract)

107. Li, X.H.; Liu, D.Y.; Sun, M. Precise U-Pb and Sm-Nd isotopic dating of the supergiant Shizhuyuan polymetallic deposit and its host granite, SE China. *Geol. Mag.* **2004**, *141*, 225–231. [CrossRef]
108. Li, H.Y.; Mao, J.W.; Sun, Y.L.; Zou, X.Q.; He, X.L.; Du, A.D. Re-Os isotopic chronology of molybdenites in Shizhuyuan polymetallic tungsten deposit. *Geol. Rev.* **1996**, *42*, 261–267. (In Chinese with English abstract)